Surface Organozirconium Electrophiles Activated by Chemisorption on "Super Acidic" Sulfated Zirconia as Hydrogenation and Polymerization Catalysts. A Synthetic, Structural, and Mechanistic Catalytic Study

Hongsang Ahn, Christopher P. Nicholas, and Tobin J. Marks*

Department of Chemistry, Northwestern University, 2145 Sheridan Road, Evanston, Illinois 60208-3113

Structural studies including ^{13}C CPMAS NMR spectroscopy of the $^{13}C_\alpha$-enriched model adsorbates $Cp'_2Th(^{13}CH_3)_2$ (**1***) and $CpTi(^{13}CH_3)_3$ (**2***) ($Cp = \eta^5\text{-}C_5H_5$, $Cp' = \eta^5\text{-}(CH_3)_5C_5$), and organozirconium adsorbates $Cp_2Zr(^{13}CH_3)_2$ (**3***), $Cp'Zr(^{13}CH_3)_3$ (**4***), and $Zr(^{13}CH_2tBu)_4$ (**6***) chemisorbed on superacidic sulfated zirconia (ZRSx; x = activation temperature) reveal that all adsorbates undergo a new molecular chemisorptive process: protonolytic M−C σ-bond cleavage at the very strong surface Brønsted acid sites to yield "cation-like" organometallic electrophiles. A kinetic and mechanistic study is reported for olefin and arene hydrogenation and α-olefin homopolymerization mediated by the catalysts formed by chemisorption of Cp_2-$Zr(CH_3)_2$ (**3**), $Cp'Zr(CH_3)_3$ (**4**), $Zr(CH_2TMS)_4$ (**5**), $Zr(CH_2tBu)_4$ (**6**), and $Zr(CH_2Ph)_4$ (**7**), onto zirconia (ZR) or ZRSx. At 25 °C, 14.7 psi H_2, 1-hexene hydrogenation activity follows the order **4**/ZRS400 ≫ **3**/ZRS400 ≥ **3**/ZRS300 ≫ **3**/ZRS720 ≫ **3**/ZR ∼ 0. Benzene hydrogenation rates (25 °C, 14.7 psi H_2) follow the order **4**/ZRS400 ≫ **5**/ZRS400 > **6**/ZRS400 > **7**/ZRS400, with $N_t = 970$ h^{-1} for **4**/ZRS400 making this the most active benzene hydrogenation catalyst yet discovered. As a function of arene substituent(s), **4**/ZRS400 exhibits high chemoselectivity, with hydrogenation rates following the order benzene ≫ toluene ≫ *p*-xylene ∼ 0. For benzene hydrogenation by **6**/ZRS400, kinetic data obey the rate law $N_t = k_{obs}[\text{arene}]^0[P_{H_2}]^1$ with $E_a = 10.3(8)$ kcal mol^{-1}. Partially hydrogenated products are not detected at partial conversions, with H_2 delivered pairwise to both faces of C_6D_6, forming all-*cis* and *cis, cis, trans, cis, trans* isotopomers (1:3.1). Protonolytic poisoning experiments reveal that a maximum of ∼68% of Zr sites in **4**/ZRS400 are catalytically significant for benzene hydrogenation. Relative homopolymerization rates are **7**/ZRS400 > **5**/ZRS400 > **6**/ZRS400 > **4**/ZRS400 for both ethylene (150 psi C_2H_4, 60 °C) and liquid propylene (20 °C).

Introduction

Chemisorptive interactions of metal−organic complexes with metal oxide surfaces have been of great recent interest due to the exceptional reactivity and catalytic activity exhibited by the resulting adsorbate species.[1] Although conventional heterogeneous Ziegler−Natta catalysis and related precesses have been of great scientific and technological interest, it was not until the recent development of homogeneous single-site polymerization catalysis[2] that heterogeneous polymerization research could fully elucidate the origins of reactivity and create new generations of supported catalysts by tailoring the molecular structures of the adsorbate
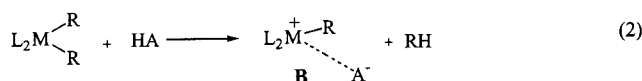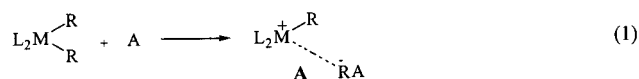
precatalysts.[3] Recent studies of homogeneous Ziegler−Natta catalysis show that highly electrophilic "cationic" complexes (**A** and **B**; L = ancillary ligand) are the catalytically active species. Such "cationic" species can

(1) (a) Sheldon, R. A., van Bekkum, H., Eds. *Fine Chemicals through Heterogeneous Catalysis*; Wiley-VCH: Weinheim, 2001. (b) Lindner E.; Auer F.; Baumann A.; Wegner P.; Mayer H. A.; Bertagnolli H.; Reinohl U.; Ertel T. S.; Weber A, *J. Mol. Catal. A-Chem.* **2000**, *157* (1−2), 97−109. (c) Lefebvre, F.; Basset, J. M. *J. Mol. Catal. A-Chem.* **1999**, *146* (1−2), 3−12. (d) Scott, S. L.; Basset, J.-M.; Niccolai, G. P.; Santini, C. C.; Candy, J. P.; Lecuyer, C.; Quignard, F.; Choplin, A. *New J. Chem.* **1994**, *18*, 115−122. (e) Iwasawa, Y.; Gates, B. C. *Chemtech* **1989**, *3*, 173−181, and references therein. (f) Basset, J.-M., et al., Eds. *Surface Organometallic Chemistry: Molecular Approaches to Surface Catalysis*; Kluwer: Dordrecht, 1988. (g) Iwasawa, Y. *Adv. Catal.* **1987**, *35*, 187−264. (h) Hartley, F. R. *Supported Metal Complexes: A New Generation of Catalysts*: Reidel: Boston, 1985.

(2) (a) Chen, E. Y.-X.; Marks, T. J. *Chem. Rev.* **2000**, *100* (4), 1391−1434. (b) Gladysz, J. A., Ed. *Chem. Rev.* **2000**, *100* (special issue on "Frontiers in Metal-Catalyzed Polymerization"). (c) Marks, T. J., Stevens, J. C., Eds. *Top. Catal.* **1999**, *7*, 1 (special volume on "Advances in Polymerization Catalysis. Catalysts and Processes"). (d) Kaminsky, W. *Metalorganic Catalysts for Synthesis and Polymerization: Recent Results by Ziegler-Natta and Metallocene Investigations*; Springer-Verlag: Berlin, 1999. (e) Britovsek, G. J. P.; Gibson, V. C.; Wass, D. F. *Angew. Chem., Int. Ed. Engl.* **1999**, *38*, 428−447. (f) Jordan, R. F. *Metallocene and Single Site Olefin Catalysis. J. Mol. Catal.* **1998**, *128* (special issue), and references therein. (g) Kaminsky, W.; Arndt, M. *Adv. Polym. Sci.* **1997**, *127*, 144−187. (h) Bochmann, M. *J. Chem. Soc., Dalton Trans.* **1996**, 255−270. (i) Brintzinger, H. H.; Fischer, D.; Mülhaupt, R.; Rieger, B.; Waymouth, R. M. *Angew. Chem., Int. Ed. Engl.* **1995**, *34*, 1143−1170. (j) Soga, K., Terano, M., Eds. *Catalyst Design for Tailor-Made Polyolefins*; Elsevier: Tokyo, 1994.

(3) (a) Hlatky, G. G. *Chem. Rev.* **2000**, *100* (4), 1347−1376 (b) Ribeiro, M. R.; Deffieux, A.; Portela, M. F. *Ind. Eng. Chem. Res.* **1997**, *36*, 1224−1237, and references therein. (c) Soga, K.; Kim, H. J.; Shiono, T. *Makromol. Chem. Rapid Commun.* **1994**, *15*, 139−143. (d) Janiak, C.; Rieger, B. *Angew. Makromol. Chem.* **1994**, *215*, 47−57. (e) Kaminsky, W.; Renner, F. *Makromol. Chem. Rapid Commun.* **1993**, *14*, 239−243. (f) Collins, S.; Kelly, W. M.; Holden, D. A. *Macromolecules* **1992**, *25*, 1780−1785. (g) Soga, K.; Kaminaka, M. *Makromol. Chem. Rapid. Commun.* **1992**, *13*, 221−224.

be produced using either organo-Lewis acidic (alkide/hydride abstraction; **A**, eq 1)[2,4] or Brønsted acidic (M–alkyl/H protonolysis; **B**, eq 2) cocatalyst/reagents.[2,5]

$$L_2M\underset{R}{\overset{R}{<}} \ + \ A \ \longrightarrow \ L_2\overset{+}{M}\underset{A\cdots RA}{\overset{R}{<}} \qquad (1)$$

$$L_2M\underset{R}{\overset{R}{<}} \ + \ HA \ \longrightarrow \ L_2\overset{+}{M}\underset{B\cdots A^-}{\overset{R}{<}} \ + \ RH \qquad (2)$$

Although the complex, irregular adsorption environments on oxide surfaces complicate identification and structural characterization of the active chemisorbed catalytic species (as opposed to "spectators") with the precision possible for homogeneous catalysts, supported molecular catalysts have been argued to follow similar routes to "cation-like" structures.[6] Thus, previous research from this laboratory adopted ^{13}C-enriched organoactinides such as Cp'$_2$Th([13]CH$_3$)$_2$ (**1**) [Cp' = (CH$_3$)$_5$C$_5$] and early transition metal hydrocarbyls as model adsorbates to support on dehydroxylated γ-alumina (DA; σ-OH $\approx$ 0.1 nm^{-2}), partially dehydroxylated alumina (PDA; σ-OH $\approx$ 4 nm^{-2}), silica (partially dehydroxylated or dehydroxylated; PDS or DS, respectively), MgCl$_2$, silica–alumina, and MgO.[6a,c,f–g] Solid-state ^{13}C CPMAS NMR studies identified species by comparison to the spectral signatures of homogeneous analogues and suggested that "cation-like structures" (e.g., structure **C**) are responsible for the high catalytic activity with respect to hydrocarbon transformations. Here the dotted line denotes a weak, predominantly electrostatic interaction (cf., **A** and **B**).
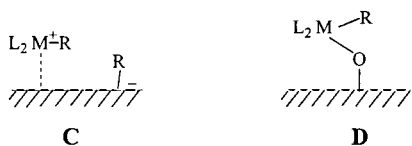
Additionally, kinetic studies,[6d,f,j] stoichiometric probe reactions,[6d,e] and poisoning experiments[6d–f,j] have elucidated catalytic rate laws, active chemical functionalities, and percentages of catalytically significant sites. In addition to establishing that strong Lewis acidic surfaces (DA, PDA, MgCl$_2$) can activate metallocenes via heterolytic M–C scission, i.e., transferring an alkide group to surface Lewis acid sites (structure **C**), it was shown that on conventional weakly Brønsted acidic surfaces (PDS, MgO), μ-oxo structures are produced via M–CH$_3$ protonolysis (structure **D**) and that these are chemically inert, in agreement with the properties of solution phase analogues.[6e,h]

Recently, sulfated zirconia (ZRSx; x = the activation temperature) and related solid acids[7] have received considerable attention owing to their unusual ambient temperature hydrocarbon transformation activities.[8] While many groups have intensively studied the structure of the ZRSx active site(s),[9] acidity characteristics,[10] and surface modifications with other metal oxides,[11] many aspects of sulfated zirconia structure and function remain unresolved. We initiated the present study with the goals of (1) characterizing intrinsic interactions of metal hydrocarbyls with very strong Brønsted acid surface sites (as opposed to previous work with weak Brønsted acids), (2) defining the structures of the resulting adsorbate molecules, and (3) developing new molecule-derived supported catalysts for hydrocarbon transformations and olefin polymerization.

With these objectives in mind, this contribution presents detailed discussions of the (1) characterization of Cp$_2$ZrR$_2$, Cp'ZrR$_3$, and ZrR$_4$–ZRSx surface interaction modes and active site structures by various spectroscopic techniques, including high-resolution solid-state ^{13}C NMR spectroscopy, using model adsorbates and actual catalysts, (2) the scope, regiochemistry, kinetics, and mechanisms of α-olefin and arene hydrogenation, and (3) olefin homopolymerization mediated by these ZRSx-supported catalysts. It will be seen that this approach of integrating spectroscopy, chemisorption, and mechanistic catalysis affords unique insight into the nature of these molecule-derived surface electrophiles, several of which exhibit exceptional catalytic activity.

Experimental Section

All synthetic procedures were carried out in Schlenk-type glassware interfaced to a high-vacuum (10^{-5}–10^{-6} Torr) line

(4) (a) Chen, Y.-X.; Metz, M. V.; Li, L.; Stern, C. L.; Marks, T. J. *J. Am. Chem. Soc.* **1998**, *120*, 6287–6305. (b) Deck, P. A.; Beswick, P. A.; Marks, T. J. *J. Am. Chem. Soc.* **1998**, *120*, 1772–1784. (c) Sun, Y.; Spence, R. E. V. H.; Piers, W. E.; Parvez, M.; Yap, G. P. A. *J. Am. Chem. Soc.* **1997**, *119*, 5132–5143, and references therein. (d) Baumann, R.; Davis, W. M.; Schrock, R. R. *J. Am. Chem. Soc.* **1997**, *119*, 3830–3831. (e) Wang, Q.; Gillis, D. J.; Quyoum, R.; Jeremic, D.; Tidoret, M.-J.; Baird, M. C. *J. Organomet. Chem.* **1997**, *527*, 7–14. (f) Chen, Y.-X.; Stern, C. L.; Yang, S.; Marks, T. J. *J. Am. Chem. Soc.* **1996**, *118*, 12451–12452. (g) Yang, X.; Stern, C. L.; Marks, T. J. *J. Am Chem. Soc.* **1994**, *116*, 10015–10031.

(5) (a) Giardello, M. A.; Eisen, M. S.; Stern, C. L.; Marks, T. J. *J. Am. Chem. Soc.* **1995**, *117*, 12114–12129. (b) Jia, L.; Yang, X.; Stern, C. L.; Marks, T. J. *Organometallics* **1994**, *13*, 3755–3757. (c) Hlatky, G. G.; Eckman, R. R.; Turner, H. W. *Organometallics* **1992**, *11*, 1413–1416. (d) Yang, X.; Stern, C. L.; Marks, T. J. *Organometallics* **1991**, *10*, 840–842. (e) Turner, H. W.; Hlatky, G. G. PCT Int. Appl. WO 88/05793 (Eur. Pat. Appl. EP 211004, 1988).

(6) (a) Ahn, H.; Marks, T. J. *J. Am. Chem. Soc.* **1998**, *120* (51), 13533–13534 (preliminary communication of some aspects of this work). (b) Eisen, M. S.; Marks, T. J. *J. Mol. Catal.* **1994**, *86*, 23–50. (c) Marks, T. J. *Acc. Chem. Res.* **1992**, *25*, 57–65. (d) Eisen, M. S.; Marks, T. J. *J. Am. Chem. Soc.* **1992**, *114*, 10358–10368. (e) Finch, W. C.; Gillespie, R. D.; Hedden, D.; Marks, T. J. *J. Am. Chem. Soc.* **1990**, *112*, 6221–6232. (f) Gillespie, R. D.; Burwell, R. L., Jr.; Marks, T. J. *Langmuir* **1990**, *6*, 1465–1477. (g) Dahmen, K. H.; Hedden, D.; Burwell, R. L., Jr.; Marks, T. J. *Langmuir* **1988**, *4*, 1212–1214. (h) Toscano, P. J.; Marks, T. J. *Langmuir* **1986**, *2*, 820–823. (i) Toscano, P. J.; Marks, T. J. *J. Am. Chem. Soc.* **1985**, *107*, 653–659. (j) He, M.-Y.; Xiong, G.; Toscano, P. J.; Burwell, R. L. Jr.; Marks, T. J. *J. Am. Chem. Soc.* **1985**, *107*, 641–652. (k) He, M.-Y.; Burwell, R. L. Jr.; Marks, T. J. *Organometallics* **1983**, *2*, 566–569.

(7) For recent reviews, see: (a) Song, X.; Sayari, A. *Catal. Rev.-Sci. Eng.* **1996**, *38* (3), 329–412, and references therein. (b) Corma, A. *Chem. Rev.* **1995**, *95*, 559–614. (c) Arata, K. *Adv. Catal.* **1990**, *37*, 165–211.

(8) (a) Jin, T.; Yamaguchi, T.; Tanabe, K. *J. Phys. Chem.* **1986**, *90*, 4794–4796. (b) Hino, M.; Kobayashi, S.; Arata, K. *J. Am. Chem. Soc.* **1979**, *101*, 6439–6441.

(9) (a) Kustov, L. M.; Kazansky, V. B.; Figueras, F.; Tichit, D. *J. Catal.* **1994**, *150*, 143–149. (b) Clearfield, A.; Serrette, G. P. D.; Khazi-Syed, A. H. *Catal. Today* **1994**, *20*, 295–312. (c) Riemer, T.; Spielbauer, D.; Hunger, M.; Mekhemer, G. A. H.; Knözinger, H. *J. Chem. Soc., Chem. Commun.* **1994**, 1181–1182. (d) Bensitel, M.; Saur, O.; Lavalley, J. C.; Morrow, B. A. *Mater. Chem. Phys.* **1988**, *19*, 147–156.

(10) (a) Spielbauer, D.; Mekhemer, G. A. H.; Zaki, M. J.; Knözinger, H. *Catal. Lett.* **1996**, *40*, 71–79. (b) Adeeva, V.; de Han, J. W.; Jänchen, J. Lei, G. D.; Schünemann, V.; van de Ven, L. J. M.; Sachtler, W. M. H.; van Santen, R. A. *J. Catal.* **1995**, *151*, 364–372. (c) Matsuhashi, H.; Motoi, H.; Arata, K. *Catal. Lett.* **1994**, *26*, 325–328.

(11) (a) Canton, P.; Olindo, R.; Pinna, F.; Strukul, G.; Riello, P.; Meneghetti, M.; Cerrato, G.; Morterra, C.; Benedetti, A. *Chem. Mater.* **2001**, *13* (5), 1634–1641. (b) Matsuhashi, H.; Tanaka, M.; Nakamura, H.; Arata, K. *Appl. Catal., A* **2001**, *208* (1, 2), 1–5. (c) Xia, Q.-H.; Hidajat, K.; Kawi, S. *J. Chem. Soc., Chem. Commun.* **2000**, *22*, 2229–2230.

or in a nitrogen-filled Vacuum Atmospheres glovebox (0.5–1.0 ppm O_2). Argon (Matheson) and hydrogen (Matheson) were purified by passage through MnO/vermiculite and Davison 4 Å molecular sieve columns. Oxygen (Matheson) was dried by passage through Drierite (Hammond Co.). All solvents, 1-hexene (Aldrich), and arenes (Aldrich) were distilled from Na/K alloy. The organometallic complexes $Cp_2Zr(CH_3)_2$ (**3**),[12] Cp'_2-$Hf(CH_3)_2$,[13] $Cp'Zr(CH_3)_3$ (**4**)[14] [Cp = η^5-C_5H_5, Cp' = η^5-$(CH_3)_5C_5$], $Zr(CH_2TMS)_4$ (**5**)[15] [TMS = $Si(CH_3)_3$], $Zr(CH_2tBu)_4$ (**6**),[16] and $Zr(CH_2Ph)_4$ (**7**)[17] were prepared by the literature procedures. The labeled complexes $Cp'_2Th(^{13}CH_3)_2$ (**1***),[18] $CpTi(^{13}CH_3)_3$ (**2***),[19] $Cp_2Zr(^{13}CH_3)_2$ (**3***), $Cp'Zr(^{13}CH_3)_3$ (**4***), and $Zr(CH_2tBu)_4$ (**6***) were synthesized using analogous methods from $^{13}CH_3$-Li·LiI prepared from $^{13}CH_3I$ (99% ^{13}C, Cambridge Isotopes) or appropriate ^{13}C-enriched precursors (vide infra). Partially dehydroxylated silica (PDS) was prepared by heating Davison grade 62 silica gel (60–80 mesh, previously washed with 0.1 M HNO_3, and dried) at 450 °C for 12 h under high vacuum (5 × 10⁻⁶ Torr). Dehydroxylated alumina (DA, American Cyanamid γ-alumina, 99.99% purity)[6f,j] was prepared as previously described. Freshly prepared supports were stored in vacuum-tight storage tubes under inert atmosphere until used.

Synthesis of $Zr(^{13}CH_2{}^tBu)_4$ (6*). A flask of $^{13}CO_2$ (1.0 L, 1.0 atm pressure, 44.6 mmol) equipped with a break-seal and an extra outer J-Young valve was attached to a high-vacuum line. A flask containing ^tBuMgCl (25 mL of 2 M solution in ether, 50.0 mmol) was also attached to the high-vacuum line and evacuated at −78 °C. The reaction was initiated and performed in an enclosed volume of the vacuum line by using a magnet to break the break-seal of the $^{13}CO_2$ flask with a magnetic stirring bar, and the $^{13}CO_2$ was introduced into the chilled stirring solution of ^tBuMgCl. The solution was stirred at −15 °C for 12 h, and then 30 mL of distilled water and 7.0 mL of concentrated HCl were carefully syringed in at −20 °C. Two layers formed, and the ether layer was separated, while the water layer was extracted with 3 × 20 mL of ether. After drying the combined ether layers over $MgSO_4$ and filtration, the ether was removed on a rotary evaporator at 0 °C. The resulting $^tBu^{13}C(O)OH$ (yield 92%) was reduced with $LiAlH_4$ in ether at 25 °C to give $^tBu^{13}CH_2OH$ (yield, 95%). Next, the $^tBu^{13}CH_2OH$ was refluxed with Ph_3PCl_2 in DMF for 2 h, and then 20 mL of H_2O was added to afford $^tBu^{13}CH_2Cl$ (yield, 61%) after extraction with pentane. Finally, $Zr(^{13}CH_2{}^tBu)_4$ (**6***) was prepared from the $^tBu^{13}CH_2Cl$ via the corresponding lithium reagent and subsequently purified using the literature procedure.[16]

Preparation of Zirconia (ZR).[20] Aqueous ammonia was added to a stirring aqueous solution of $ZrOCl_2$ (Aldrich) until pH = 10.0. The resulting precipitate $[Zr(OH)_4]$ was then collected by filtration, dried under air at 100 °C for 12 h, and then calcined under flowing dry O_2 (100 mL/min) at 500 °C for 10 h, yielding zirconia (ZR).

Preparation of Sulfated Zirconia (ZRSx).[21] A precursor of sulfated zirconia (ZRS0) was prepared by thermal decomposition of $Zr(SO_4)_2·4H_2O$ (ZRS; 3.5 g, Aldrich, 99%) at 730 °C for 5 h in flowing O_2 (100 mL/min). Then the samples were

transferred to the vacuum line in air. Finally, the ZRS0 was activated in flowing Ar (100 mL/min) for 45 min and subsequently under high vacuum (5 × 10⁻⁶ Torr) for 75 min at 300 (ZRS300), 400 (ZRS400), or 720 (ZRS720) °C, respectively.

Chemisorption of Organometallic Complexes on Prepared Supports. In a two-sided fritted reaction vessel interfaced to the high-vacuum line, 10 mL of pentane was condensed onto well-mixed, measured quantities of the organometallic complex and support. The resulting slurry was next stirred for 1.0 h and filtered. The impregnated support was collected on the frit, washed three times with pentane, and finally dried in vacuo. The prepared catalyst was transferred to the glovebox and stored in a sealed vial in the dark at −40 °C until used.

Physical and Analytical Measurements. The following instruments were used: ^1H, ^{13}C NMR: Varian Mercury 400 and Varian INOVA 500; ^{13}C CPMAS solid-state NMR: Varian VXR300; BET/pore size distribution: Omnisorb 360; thermogravimetric analysis: TA SDT 2960; XRD: Rigaku D/MAX II; GC/MSD: Hewlett-Packard 6890; IR: Biorad FTS-60. ICP measurements were performed with a Thermo Jarrell Ash Atom Scan 25 spectrometer. The loading of the organometallic complexes and sulfur content in ZRS400 were measured by ICP after digestion of a known amount of a support or supported catalyst in a closed 60 mL Teflon vessel filled with 50% aq. HF solution at 100 °C for 12 h. IR spectra were measured under inert atmosphere using an O-ring-sealed sample holder with CaF_2 windows. ^1H and ^{13}C NMR experiments on air-sensitive solution samples were conducted in Teflon valve-sealed sample tubes (J-Young). For ^{13}C CPMAS solid-state NMR spectroscopy, air-sensitive samples were loaded into cylindrical silicon nitride rotors in the glovebox with O-ring-sealed Kel-F caps. Typically, a spinning rate of 6.3 kHz could be achieved with a Doty Scientific 5 mm supersonic probe using boil-off nitrogen as the spinning gas to prevent sample exposure to air. Since the samples are extremely air- and moisture-sensitive, rotors were loaded and packed with catalyst samples inside the glovebox under an anaerobic nitrogen atmosphere. When samples were deliberately exposed to air, no spectral features were detectable. All solid-state ^{13}C NMR spectra were externally referenced to adamantane by assigning its major resonance at δ 37.7. In general, 8000–10 000 scans were employed to obtain satisfactory spectra of the supported organometallic samples. GPC data on all polymer samples were recorded on a Waters Alliance GPCV 2000 relative to polystyrene standard.

Olefin/Arene Hydrogenation and Kinetic Studies. Catalytic hydrogenation and kinetic studies were performed with the two different types of reactors described below.

Reactor A.[22] Typical reactions were carried out in a constant volume, pseudo-constant-pressure gas uptake apparatus equipped with a Barocel differential manometer to measure small pressure changes between the gas ballasts.[23] The glass reaction vessel (∼10 mL in volume) was fitted with Morton-type indentations and a high-speed vortex agitator (American Scientific MT-51 vortex mixer) to ensure efficient mixing, a water jacket connected to a recirculating pump, a Haake constant-temperature bath (25.0(1) °C), calibrated burets for admitting reagents, and a large diameter flexible stainless steel connection to a high-vacuum line. The gas handling system was interfaced to two 500 mL gas ballasts (all thermostated at 25.0(1) °C). In a typical experiment, the reaction vessel was dried under high-vacuum (5 × 10⁻⁷ Torr) for >2 h and taken into the glovebox, the catalyst was introduced into the reaction chamber, and the substrates were introduced into the burets. The vessel was then transferred

(12) Wailes, P. C.; Weigold, H.; Bell, A. P. *J. Organomet. Chem.* **1972**, *34*, 105–164.

(13) Smith, G. M. Ph.D. Thesis, Northwestern University, Evanston, IL, 1987.

(14) Wolczanski, P. T.; Bercaw, J. E. *Organometallics* **1982**, *1*, 793–799.

(15) Collier, M. R.; Lappert, M. F.; Pearce, R. *J. Chem. Soc., Dalton Trans.* **1973**, 445–451.

(16) Davidson, P. J.; Lappert, M. F.; Pearce, R. *J. Organomet. Chem.* **1973**, *57*, 269–277.

(17) Zucchini, U.; Albizzati, E.; Giannini, U. *J. Organomet. Chem.* **1971**, *26*, 357–372.

(18) Fagan, P. J.; Manriquez, J. M.; Maatta, E. A.; Seyam, A. M.; Marks, T. J. *J. Am. Chem. Soc.* **1981**, *103*, 6650–6667.

(19) Giannini, U.; Cesca, S. *Tetrahedron Lett.* **1960**, *14*, 19–20.

(20) Vera R. C.; Parera, J. M. *J. Catal.* **1997**, *165*, 254–262.

(21) Platero, E. E.; Mentruit, M. P. *Catal. Lett.* **1995**, 31–39.

(22) See Supporting Information.

(23) (a) Roesky, P. W.; Denninger, U.; Stern, C. L.; Marks, T. J. *Organometallics* **1997**, *16*, 4486–4492. (b) Haar, C. M.; Stern, C. L.; Marks, T. J. *Organometallics* **1996**, *15*, 1765–1784.

outside to the vacuum line, evacuated, and filled with H_2 (1.0 atm). Next, the thermostated water circulating system was connected and actuated. The substrate was then introduced, and the valve between the ballasts closed. Vortex mixing was then initiated (>2000 rpm), and the H_2 pressure was recorded as a function of time. Poisoning experiments were carried out by titrating measured quantities of degassed H_2O in C_6D_6[6d] into the reactor and measuring the catalytic activity after each addition. Active site calculations were based on the reasonable assumption that each molecule of H_2O undergoes reaction with/poisons 1.0 active site.

Reactor B.[22] In a typical experiment, a 60 mL Griffin-Worden quartz medium-pressure reactor (Kontes Corp., Vineland, NJ) connected to a 500 mL metal gas ballast tank was flamed under high vacuum and charged in the glovebox with a measured amount (50 mg) of heterogeneous catalyst and 1.0 mL (1.1×10^{-2} mol) of benzene dried over Na/K. The apparatus was removed from the glovebox and attached to the high-vacuum line. After thorough evacuation (10^{-5} Torr) of the reactor at −78 °C, the reactor was warmed to room temperature and pressurized to 190 psi of H_2. The reactor was then immersed in a oil bath maintained at 90(0.1) °C or at the desired temperature and stirred rapidly (>1500 rpm). The consumption of H_2 was measured with an Omega PX425-300GV digital pressure transducer.

Kinetic Measurements. Reactors A and B, which enable accurate constant volume and pseudo-constant pressure gas uptake measurements, were used for all kinetic experiments. The change of H_2 pressure during any kinetic run was always maintained at less than 10% of the system pressure (pseudo-zero-order in P_{H_2}). All kinetic experiments were carried out under rapid mixing conditions, which were established in control experiments to be beyond the H_2 mass transfer limit.

Ethylene and Propylene Homopolymerization Experiments. Ethylene (Matheson) and propylene (Matheson) were purified by oxygen/moisture traps (Matheson, model 6427-2S). The supported catalyst was charged into a high-pressure quartz reactor interfaced to the high-vacuum line; 5 mL of dry toluene was introduced, followed by charging with ethylene to the desired pressure (ethylene homopolymerization), or with propylene, which was condensed into the reactor at −78 °C. After warming to room temperature, the slurry was rapidly stirred (>1500 rpm). After a measured time interval, the polymerization was quenched with methanol, and the polymeric product was collected by filtration, dried overnight under high vacuum at 80 °C, and weighed.

Results

We begin by discussing the synthesis and characterization of precatalysts and supports (ZRSx, ZR), followed by ^{13}C CPMAS NMR spectroscopic analysis of Cp$'_2$Th-($^{13}CH_3$)$_2$ (**1***) and CpTi($^{13}CH_3$)$_3$ (**2***) as "model" adsorbates on ZRS400, and then correlate the results with those on DA, DS, or PDS. We then employ the actual zirconium precatalysts Cp$_2$Zr($^{13}CH_3$)$_2$ (**3***), Cp$'$Zr($^{13}CH_3$)$_3$ (**4***), and Zr($^{13}CH_2{}^tBu$)$_4$ (**6***) as labeled adsorbates in CPMAS NMR studies. In previous reports, the spectra of the complexes **1*** and **3*** supported on various dehydroxylated or partially dehydroxylated supports (i.e., DA, DS, and PDS) were thoroughly analyzed.[6c,e,g−i] On this basis, we then analyze the generality and the specificity of ZRSx surface organometallic interactions for complexes **1***, **2***, **3***, **4***, and **6*** (Table 1). Reactivity patterns are seen to differ dramatically from those on weak Brønsted acid surfaces. Next, we discuss catalytic 1-hexene hydrogenation mediated by these species, and then arene hydrogenation, focusing on rate and active site count, as well as kinetics as a function of H_2
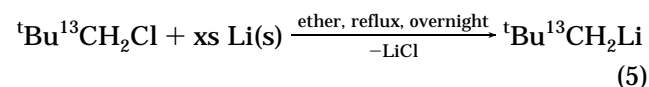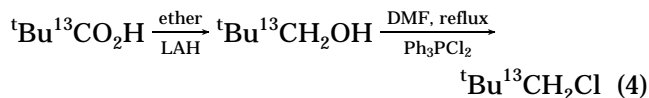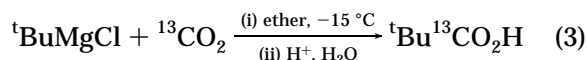
pressure and temperature for several selected catalysts. Finally, we analyze ethylene and propylene homopolymerization processes mediated by **4**/ZRS400, **5**/ZRS400, **6**/ZRS400, and **7**/ZRS400 and the characteristics of the resulting polymers.

I. Catalyst Preparation and Characterization. (A) Precatalyst and Support Synthesis. All organometallic catalyst precursors used in this study were prepared as described elsewhere.[12−16] To probe the effects of the precatalyst coordinative saturation on catalytic characteristics, zirconium bis(cyclopentadienyl) (**E**), mono(cyclopentadienyl) (**F**), and tetrakis(hydrocarbyl) (**G**) complexes were examined. Methyl group ^{13}C
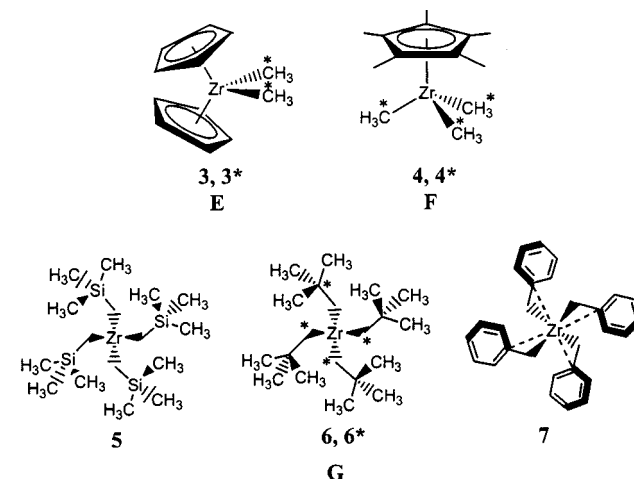
enrichment in complexes **3** and **4** (**3***, **4***) was readily achieved with 99% ^{13}C-enriched $^{13}CH_3Li$. The α-^{13}C-enriched tetrakis(neopentyl zirconium) precatalyst (**6***) was prepared from $^tBu^{13}CH_2Li$ (eqs 3−5), followed by the reaction of ZrCl$_4$ with $^tBu^{13}CH_2Li$, in turn prepared by lithiation of $^tBu^{13}CH_2Cl$.

$$^tBuMgCl + {}^{13}CO_2 \xrightarrow[\text{(ii) } H^+, H_2O]{\text{(i) ether, } -15\,°C} {}^tBu^{13}CO_2H \quad (3)$$

$$^tBu^{13}CO_2H \xrightarrow{\text{ether}}_{\text{LAH}} {}^tBu^{13}CH_2OH \xrightarrow{\text{DMF, reflux}}_{\text{Ph}_3PCl_2} {}^tBu^{13}CH_2Cl \quad (4)$$

$$^tBu^{13}CH_2Cl + \text{xs Li(s)} \xrightarrow{\text{ether, reflux, overnight}}_{-\text{LiCl}} {}^tBu^{13}CH_2Li \quad (5)$$

Several preparative methods for sulfated zirconia (notation: ZRSx where x = the activation temperature) have been reported.[7] In the present work, the Zr(SO$_4$)· 4H$_2$O thermolysis procedure[21] was the preferred method to prepare sulfated zirconia. ZRS0 thermogravimetric analysis indicates significant sulfate desorption at ≥720 °C.[22] For the present ZRS400 prepared by Zr(SO$_4$)$_2$· 4H$_2$O thermolysis, the BET surface area was found to be 110 m^2/g and the most frequent pore radius 3.5 nm (N$_2$ desorption method), while for zirconia (ZR), the BET surface area is 44 m^2/g. For the present ZRSx samples, all infrared-active O−H and S−O stretching transitions[22] were found to depend on activation temperature in a manner identical to the previous work of Platero et al.[21] Thus, IR spectra of all sulfated zirconia samples

Table 1. Solid-State ^{13}C NMR Chemical Shift Data for Neat and Supported Organometallic Complexes[a]

complex[b]	Cp or Cp′ ring	M−$^{13}C_\alpha$	Cp′−CH_3	others
Cp′$_2$Th(^{13}CH$_3$)$_2$ (**1**)[c]	123.1	68.4	12.0	
1*/DS[d]	124.2	59.0	9.2	
1*/DA[c]	124.2	71.0	10.2	−12 (Al−CH$_3$)
1*/ZRS400	127.0	72.8[e], 55(br)[f]	10.2	
CpTi(^{13}CH$_3$)$_3$(**2***)[f]	113.7	62.9		
2*/PDS	115.0	57.0[e], 45(br)[g]		
2*/ZRS400	115.4	75.5,	56(br)[e]	
Cp$_2$Zr(^{13}CH$_3$)$_2$ (**3***)[f]	111.0	31.4		
3*/PDS	111.0	22.2		
3*/DA	113.1	37.1		−11 (Al−CH$_3$)
3*/ZR	112.7	25(br)		
3*/ZRS400	113.1	37.0		
Cp′Zr(^{13}CH$_3$)$_3$ (**4***)	119.1	46.4	11.6	
4*/ZRS400	123.0	53.0, 44(sh)	9.0	
Zr(^{13}CH$_2$tBu)$_4$ (**6***)		103.0		35.3 (C$_\gamma$)
6*/PDS		94.7, 87(br)[g]		33.5 (C$_\gamma$)
6*/ZRS400		105(br), 95, 86.2		34.7 (C$_\gamma$), 32.3 (C$_\beta$)

[a] In ppm downfield from Me$_4$Si, referenced to the solid state ^{13}C spectrum of admantane (see Experimental Section for details). [b] For abbreviations, see text. [c] From ref 6h. [d] From ref 6g. [e] Assigned to C$_\alpha$ of μ-oxo metal hydrocarbyl. [f] Measured from the solution in C$_6$D$_6$. [g] Assigned to C$_\alpha$ of di-μ-oxo metal hydrocarbyl.

(ZRS300, ZRS400, ZRS720) exhibit strong, IR-active S= O stretching bands (1395 cm^{-1}). In the ν_{OH} region, the following features are also evident: (1) ZRS300 exhibits three bands, 3758, 3650, and 3300 cm^{-1} (br); (2) ZRS400 exhibits two bands at 3650 and 3300 cm^{-1} (br); (3) ZRS720 exhibits no identifiable ν_{OH} bands. Although the exact structures of sulfated zirconia acid sites are still under debate, a number of plausible structures relevant to the present discussion have been proposed on the basis of spectroscopic and small molecule adsorption techniques.[9] The band at 3758 cm^{-1} is assigned to "weakly acidic sites", having terminal Zr−OH groups (structure **H**).[9] The band at 3650 cm^{-1} is assignable to

H   **I**   **J**
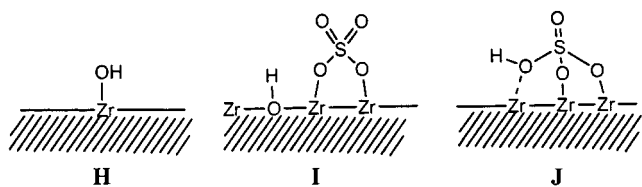
bridged hydroxyl groups,[9a] the acidity of which has been claimed to be either "weakly acidic"(structure **I**)[9a,24] or "strongly acidic" (structures **J**, **K**, **L**).[9b,10b,21] Bisulfate species (structures **K**, **L**) were also suggested to be responsible for the broad band at 3300 cm^{-1}.[9a] Recently, it was reported that these Brønsted acid sites are converted to Lewis acid sites (structure **M**; claimed to be "weakly acidic"[25]) via dehydration during calcination.[26] From these results, ZRS400 contains both strong Brønsted and Lewis acid sites, ZRS300 contains strong and weak Brønsted and Lewis acid sites, and ZRS720 contains mostly Lewis sites.

* Lewis acidic site

K   **L**   **M**
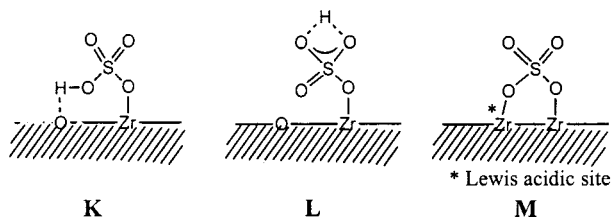
The crystal structure of sulfated zirconia is reported to be composed of monoclinic and tetragonal phases, while zirconia is mainly monoclinic.[7] It has been re-

ported that the "superacidic" properties, e.g., hydrocarbon transformations, are correlated with the population of the tetragonal phase.[27] The tetragonal phase population is quantifiable from the ratio of the X-ray power diffraction reflection intensities (eq 6):[28]

$$P_T = \frac{I(111)_T}{I(111)_T + 1.6\,I(11\bar{1})_M} \tag{6}$$

From this relationship, the tetragonal phase population, P_T, of the present ZRS400 is ~40%, while in ZR it is less than 5% (see diffraction data in Supporting Information). The above data reveal that the sulfated zirconias used in the present study for chemisorption and prepared from Zr(SO$_4$)$_2$·4H$_2$O thermolysis, have surface structural features analogous to those reported for other "superacidic" sulfated zirconias.

(B) Chemisorption Studies. Supported organometallic catalysts were prepared by exposing ZRSx to measured quantities of the complex of interest (0.81 Zr/ nm^2) in pentane solution at room temperature for 1.0 h. The resulting catalyst was then collected by filtration and washed by Soxhlet extraction with pentane at room temperature to remove any physisorbed metal hydrocarbyl. The quantity of metal hydrocarbyl and sulfur present on the support after the chemisorption process was determined (±1%) by digesting ZRS 400 samples impregnated with Cp′$_2$HfMe$_2$ as the model adsorbate using 48% aqueous HF solution and then measuring the Hf and S content by ICP spectroscopy. The organohafnium loading was determined to be 0.81 Hf/nm^2 and the S content ~3.55 S/nm^2. After chemisorbing the complexes Zr(CH$_2$^{t}Bu)$_4$ (**6**) and Zr(CH$_2$Ph)$_4$ (**7**) on sulfated zirconia in pentane slurry reactions, only neopetane (1.3 neopentane per Zr) or toluene is detected (1.1 toluene per Zr) by ^{1}H NMR spectroscopy, which

(24) Armendariz, H.; Sierra, C. S.; Figueras, F.; Coq, B.; Mirodatos, C.; Lefebvre, F.; Tichit, D. *J. Catal.* **1997**, *171*, 85−92.
(25) Morterra, C.; Cerrato, G.; Bolis, V.; Di Ciero, S.; Signoretto, M. *J. Chem. Soc., Faraday Trans.* **1997**, *93*, 1179−1184.
(26) Song, S. X.; Kydd, R. A. *J. Chem. Soc., Faraday Trans.* **1998**, *94*, 1333−1338, and references therein.
(27) Fǎrcaşiu, D.; Li, J. Q. *Appl. Catal. A-Gen.* **1995**, *128*, 97−105, and references therein.
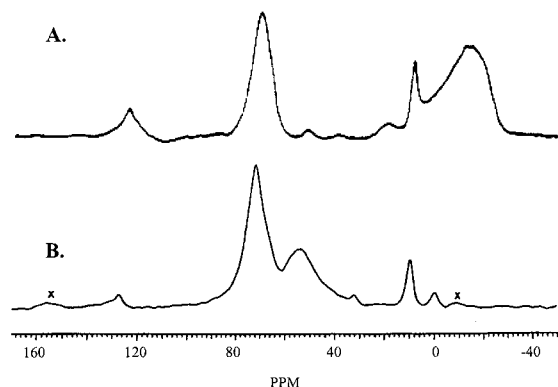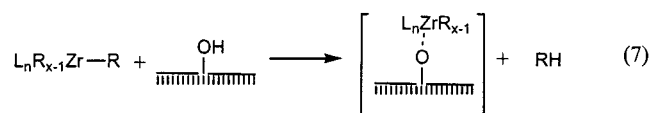(28) Corma, A.; Fornes, V.; Juan-Rajadell, M. I.; Neito, J. M. L. *App. Catal. A: Gen.* **1994**, *116*, 151−163.

A.

B.

160   120   80   40   0   -40
PPM

Figure 1. ^{13}C CPMAS NMR spectra of (A) $Cp'_2Th(^{13}CH_3)_2$-(**1***)/DA (13200 scans, repetition time = 4 s, contact time = 4.5 ms, spinning speed = 5.1 kHz; from ref 6e) and (B) **1***/ZRS400 (3430 scans, repetition time = 2.5 s, contact time = 7.1 ms, spinning speed = 6.3 kHz).

indicates that the Brønsted acidic sites effect protonolysis of one or more Zr−R σ-bonds (eq 7).

$$L_nR_{x-1}Zr{-}R + \overset{OH}{\underset{\text{surface}}{|}} \longrightarrow \left[\begin{array}{c} L_nZrR_{x-1} \\ \overset{\cdot}{O} \\ \underset{\text{surface}}{|} \end{array} \right] + RH \qquad (7)$$

After impregnation of $Cp'Zr(CH_3)_3$ (**4**) on ZRS400, the support ν_{O-H} transitions[9a,10b,21,24] at 3650 and 3300 cm^{-1} in the infrared completely disappear, and aliphatic ν_{C-H} transitions (2890−2930 cm^{-1}) appear, accompanied by a shift of $\nu_{S=O}$ from 1395 to 1360 cm^{-1}, suggesting some interaction between the (S=O)$_{surface}$ functionalities and the resulting cationic adsorbate complex (e.g., structure **N**).[22] Furthermore, IR analysis after olefin hydrogenation experiments[22] reveals that the ν_{C-H} transition is attenuated, and a new transition around 1654 cm^{-1} appears which is assignable to Zr−H stretching, reasonably produced via Zr−CH$_3$ hydrogenolysis.[4g,22,29]

$$L_nX_{x-1}Zr^+ \cdots O$$
$$\underset{\text{surface}}{S{=}O}$$

N
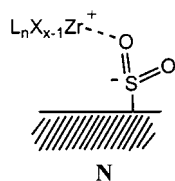
(C) ^{13}C CPMAS NMR Spectroscopic Analysis. (i) NMR Spectroscopy of Model Adsorbates Derived from Complexes 1* and 2*. Initially, model compounds $Cp'_2Th(^{13}CH_3)_2$ (**1***) and $CpTi(^{13}CH_3)_3$ (**2***) were employed as test adsorbates because (i) the relatively low-field chemical shifts of labeled Th−CH$_3$ and Ti−CH$_3$ resonances allow detection of structure-sensitive band(s) in the δ 20−40 region, which might be obscured by other major bands in the case of analogous organozirconium complexes, (ii) they are excellent pre-catalysts,[2b,6c,f,30] and (iii) for complex **1***, the results of previous surface chemistry on various supports[6c,e,h,i] can be applied to characterizing the present support−adsorbate system. The 75.4 MHz ^{13}C CPMAS spectrum of $Cp'_2Th(^{13}CH_3)_2$ (**1***)/DA is shown in Figure 1A.[6e] The low-field shift (δ 71.0; Table 1) of the labeled methyl signal can be assigned to a "cation-like" Th$^+$−CH$_3$ functionality [cf., δ 71.8 in crystallographically charac-

terized $Cp'_2Th(CH_3)^+B(C_6F_5)_4^-]^{31}$ and the upfield signal to the product of methide abstraction to yield an $^{27}Al-$CH$_3$ surface functionality (eq 1, structure **O**). Assignment of Cp' ring and methyl signals follows from data on model compounds.[6i]

O   **P**
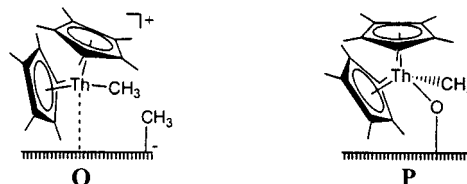
Spectra of **1***/PDA or **1***/PDS exhibit a $\delta(^{13}CH_3)$ signal at relatively high field ($\sim\delta$ 60; Table 1) and no detectable surface−CH$_3$ resonances. The former feature can be assigned to a μ-oxo species $Cp'_2Th(CH_3)O-$ on the basis of $Cp'_2Th(CH_3)OR$ model compound data (δ 58.4 for R = $CH(^tBu)_2)^{6h}$ and is reasonably derived from Th−CH$_3$ protonolysis by a residual (OH)$_{surface}$ functionality (structure **P**).[6j] These upfield spectroscopic features are quite general for early organo-transition metal and -actinide surface chemistry[6] and presumably reflect heteroatom lone pair donation to empty metal orbitals (eq 8).

$$\overset{..}{M}-\overset{..}{\underset{..}{O}}R \leftrightarrow \bar{M}{=}\overset{+}{\underset{..}{O}}R \qquad (8)$$
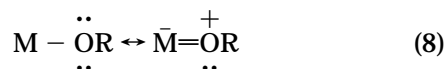
In contrast to the spectra of complex **1*** on these supports, the ^{13}C CPMAS NMR spectrum of **1*** supported on ZRS400 exhibits other characteristic features (Figure 1B). Resonances at δ 127.6 and 9.3 are assignable to the Cp' ligands, that at δ 72.8 to the labeled Th−$^{13}CH_3^+$ functionality, and the weaker band at δ 54.2 straightforwardly to a small quantity of a Th($^{13}CH_3$)O−μ-oxo species. Interestingly, δ(Th−$^{13}CH_3$) = δ 72.8 on ZRS400 is at a somewhat lower field than that associated with other "cationic" species, such as complex **1*** supported on DA or MgCl$_2$.[6e] Two weak additional resonances are observed at δ 32.6 and −0.2. Although they cannot be rigorously assigned, the chemical shifts are consistent with methide groups transferred to S$_{surface}$, i.e., S$_{surface}$−$^{13}CH_3$ (cf., HOS(O)$_2CH_3$, δ 39.4)[32] and [Zr$_{surface}$−$^{13}CH_3$], respectively. This latter upfield transferred methyl group feature agrees with those for other methylated metal oxides containing Lewis acidic sites.[6e] However, both signals are very weak in intensity compared to the Th−CH_3 resonance ($\lesssim$5%). Therefore, a "cationic" species is generated as the major adsorbate product (structure **Q**), and methide transfer to the surface is marginal on sulfated zirconia unlike chemisorption on DA and MgCl$_2$, where the intense Al$_{surface}$−

(29) Niccolai, G. P.; Basset, J.-M. *Appl. Catal.* **1996**, *146*, 145−156.
(30) (a) Liu, T. M.; Baker, W. E.; Schytt, V.; Jones, T.; Baird, M. C. *J. Appl. Polym. Sci.* **1996**, *62*, 1807−1818. For reviews, see: (b) Marks, T. J., Stevens, J. C., Eds. *Top. Catal.* **1999**, *7*, 125. (c) Tomotsu, N.; Isihara, N.; Newman, T. H.; Newman, T. H.; Malanga, M. T. *J. Mol. Catal. A* **1998**, *128* (1−3), 167−190. (d) Po, R.; Cardi, N. *Prog. Polym. Sci.* **1996**, *21*, 47−88.
(31) (a) Lin, Z.; LeMarechal, J. F.; Sabat, M.; Marks, T. J. *J. Am. Chem. Soc.* **1987**, *109*, 4127−4129. (b) Marks, T. J. *Abstracts of Papers*; 197th National Meeting of the American Chemical Society, Dallas, TX; American Chemical Society: Washington, DC, April 9−14, 1989; INOR 8.
(32) *The Aldrich Library of ^{13}C and ^1H FT NMR Spectra*, ed. I; Pouchert, C. J., Behnke, J., Eds.; Aldrich Chemical Co., Inc.: 1993.
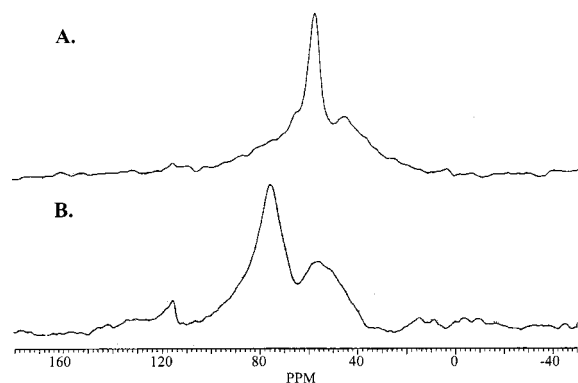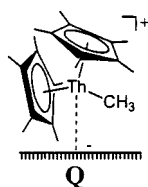
Figure 2. ^{13}C CPMAS NMR spectra of (A) CpTi(^{13}CH$_3$)$_3$-(**2***)/PDS (3750 scans, repetition time = 2.2 s, contact time = 0.2 ms, spinning speed = 6.4 kHz) and (B) **2***/ZRS400 (4200 scans, repetition time = 2.2 s, contact time = 0.2 ms, spinning speed = 4.3 kHz).

$^{13}CH_3^-$ and Mg$_{surface}$$-^{13}CH_3^-$ resonances ($\sim\delta$ −12) are almost equal in intensity to the Th$^+$−$^{13}CH_3$ signal.[6e]

Cationic complexes of the type CpTiR$_2^+$ (R = CH$_3$ or CH$_2$Ph) are highly active catalysts for producing polyethylene, polypropylene, and syndiotactic polystyrene.[2b,30] The ^{13}C CPMAS spectrum of **2***/PDS exhibits two labeled methyl peaks at δ 57.0 and 45.0 (Figure 2A) at upfield positions compared to δ 62.9 for neat complex **2**. The upfield band at δ 57.0 can be assigned to μ-oxo species Ti($^{13}CH_3$)$_2$O$^-$ (e.g., structure **R**) by analogy with surface chemistry of **1***/DS and comparison to homogeneous analogues (cf., δ 58.4 for CpTi($^{13}CH_3$)$_2$(OAr), Ar = (2,4-^{t}Bu$_2$)(6-Ph)C$_6$H$_2$).[33] Although it cannot be rigorously assigned, the marginal shoulder at δ 45.0 conceivably arises from a di-μ-oxo species, Ti($^{13}CH_3$)(O$-$)$_2$, considering the upfield displacement and the most plausible product structure deriving from protonolytic reaction between surface hydroxyl and **2***. Adsorbate **2***/ZRS400 exhibits two labeled methyl signals at δ 75.5 and 56.0 and a Cp ring carbon resonance at δ 115.4 (Figure 2B). While the feature at δ 56.0 is assignable to a μ-oxo structure (e.g., **R**) by analogy with the

2*/PDS spectrum, the band at δ 75.5 is far downfield from that of μ-oxo species or precursor **2*** (δ 62.9). It can be assigned to a "cationic" complex (e.g., **S**) by reference to homogeneous CpTi(CH$_3$)$_2^+$ complexes (cf. Cp′Ti(CH$_3$)$_2^+$Q$^-$ at δ 81.1 for Q$^-$ = (μ-CH$_3$)B(C$_6$F$_5$)$_3^-$;

CpTi(L)(CH_3)$_2^+$Q$^-$ at δ 79.97 for L = (THF)$_2$; and at δ 80.1 for L = DME, Q$^-$ = BPh$_4^-$).[34] The absence of a peak in the upfield region argues that reactions involving methide transfer to the surface are not significant as in the case of **1***/DA, but rather Ti−CH$_3$ protonolysis effected by the strong Brønsted acid surface sites dominates. These data and structural model exactly parallel that for **1***/ZRS400.[35]

In summary, the two model probe complexes **1** and **2** are primarily converted to cationic species by protonolytic chemisorption on sulfated zirconia. Additionally, methide transfer to the surface is determined to be a minor process.

(ii) NMR Spectroscopy of Organozirconium Adsorbates Derived from Precursor Complexes 3*, 4*, and 6*. ^{13}C CPMAS spectroscopic and product evolution studies of Cp$_2$Zr($^{13}CH_3$)$_2$ (**3***) and Cp′Zr-($^{13}CH_3$)$_3$ (**4***) chemisorbed on various supports have been performed and characterized vis-à-vis supported actinide hydrocarbyls.[6] In Figure 3A, the ^{13}C CPMAS spectrum of **3***/PDS exhibits the labeled methyl signal of the major surface species at relatively high field (δ 22.2), which is reasonably assigned to a μ-oxo species, Cp$_2$Zr($^{13}CH_3$)O$-$ [6a,g] (e.g., **T**), in analogy with homogeneous analogues such as Cp$_2$Zr(CH_3)OR [δ 30.8, R = CH(CH$_3$)$_2$].[36] In contrast, solid-state ^{13}C NMR data for **3***/DA (Figure 3B) consist of three bands at δ 113.1, 37.1, and −11.[6g] The band at δ 113.1 is assigned to Cp-ring carbons, the band at δ 37.1 to a "cation-like" species, Cp$_2$Zr$^{13}CH_3^+$ (structure **U**; cf., homogeneous

Figure 3. ^{13}C CPMAS NMR spectra of (A) Cp$_2$Zr($^{13}CH_3$)$_2$-(**3***)/PDS (7250 scans, repetition time = 4.0 s, contact time = 0.5 ms, spinning speed = 6.0 kHz), (B) **3***/DA (15 000 scans, repetition time = 2 s, contact time = 0.575 ms, spinning speed = 5.3 kHz), (C) **3***/ZR (8280 scans, repetition time = 1.2 s, contact time = 0.86 ms, spinning speed = 6.3 kHz), and (D) **3***/ZRS400 (9250 scans, repetition time = 1.2 s, contact time = 0.58 ms, spinning speed = 6.2 kHz).

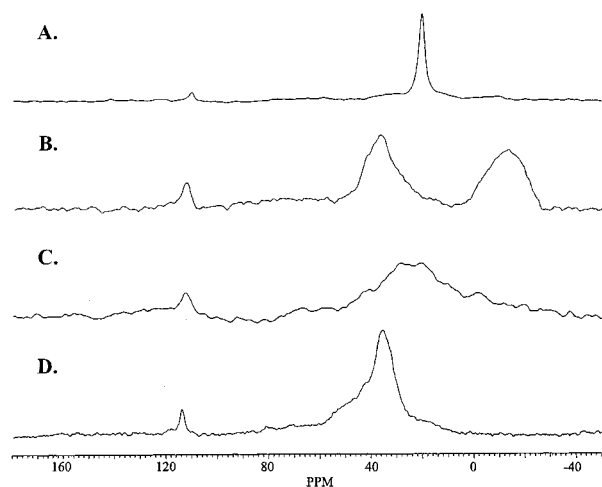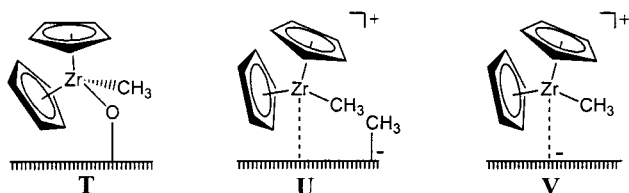(33) Thorn, M. G.; Vilardo, J. S.; Fanwick, P. E.; Rothwell, I. P. *J. Chem. Soc., Chem. Commun.* **1998**, 2427−2428.

(34) (a) Williams, E. F.; Murray, M. C.; Baird, M. C. *Macromolecules* **2000**, *33*, 261−268. (b) Bochmann, M.; Karger, G.; Jagger, A. J. *J. Chem. Soc., Chem. Commun.* **1990**, 1038−1039.

(35) Initial observations of arene hydrogenation support the "cationic" character of the catalyst **2***/ZRS400, which meditates benzene hydrogenation at 25 °C, 1.0 atm H$_2$ to yield cyclohexane with N_t = ca. 4 h^{-1}. The turnover rate frequencies for arene hydrogenation of Ti complexes supported on ZRS400 follows the order (N_t, h^{-1}): Ti(CH$_2$t-Bu)$_4$ ($\sim$7) > CpTiMe$_3$ ($\sim$ 4) > Cp′TiMe$_3$ ($\sim$1).
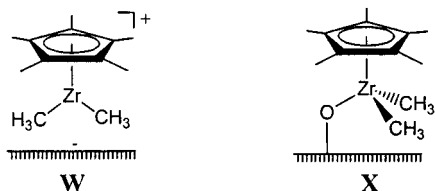
(36) Jordan, R. F.; Bagjur, C. S.; Dasher, W. E.; Rheingold, A. L. *Organometallics* **1987**, *6*, 1041−1051.

analogues, $Cp_2Zr^{13}CH_3^+Q^-$ at δ 39.8 for $Q^- = CH_3B$-$(C_6F_5)_3^-$,[4g] $Cp_2Zr(L)CH_3^+Q^-$ at δ 38.9 for L = THF[37a] and at δ 35.9 for L = 4,4′-$(CH_3)_2$-2,2′-bpy, Q^- = BPh_4^-[37b]), and a band at δ −11 to a transferred methide group analogous to that in **1***/DA (vide supra). The course of the reaction of complex **3*** with ZR is somewhat more complex, as evidenced by the ^{13}C CPMAS spectrum (Figure 3C). However, the relatively broad, relatively high-field methyl signal at δ 25 is not consistent with a "cation-like" $Cp_2Zr^{13}CH_3^+$ species, but rather is reasonably assignable to a μ-oxo species (e.g., **T**), the formation of which, without detection of a transferred methide species, argues that complex **3*** reacts protonolytically with the weakly acidic surface ZrO_2 hydroxyl functionalities.[25] Notably, this assignment is in good accord with the marginal catalytic activity (vide infra).

Figure 3D presents the ^{13}C CPMAS NMR spectrum of **3***/ZRS400. Here only two major resonances are detected at δ 113.1, assignable to the Cp ligand ring carbon, and at δ 37.0, assignable to a $Cp_2Zr^{13}CH_3^+$ species, with a small shoulder at ca. δ 20, assignable to a surface μ-oxo complex, $Cp_2Zr(^{13}CH_3)O^-$. During the chemisorption step in slurry reactions, the formation of free CpH, which would form via protonolysis of the Cp ring, was below the solution ^1H NMR detection limits. Unlike the spectrum of **3***/DA, however, a transferred methide group signal is not observable, a pattern of which was already observed for model complexes **1***/ and **2***/ZRS400. Therefore, structure **V** is analogously assigned as the major chemisorption species for **3***/ZRS400.

The spectrum of **4***/ZRS400 also exhibits two major bands and one shoulder, assignable to a Cp-ring carbon (δ 123.0), to a cationic $Cp'Zr(^{13}CH_3)_2^+$ species (δ 53.0; structure **W**), and to a μ-oxo species, $Cp'Zr(^{13}CH_3)_2O-$ (δ 44; structure **X**), respectively, with no detectable transferred surface methide signal (Figure 4A). The assigned μ-oxo species is confirmed by comparisons to the homogeneous analogues, which exhibit comparable chemical shifts (e.g., $Cp'Zr(CH_3)_2OC_6H_3(2,6$-R,R′): for R, R′ = $C(CH_3)_2$, δ 45.37; for R = CH_3, R′ = $C(CH_3)_2$, δ 41.26).[38] In regard to single-ring cationic species, the $Cp'Zr(^{13}CH_3)_2^+Q^-$ and $Cp'Zr(^{13}CH_3)_2(L)^+Q^-$ δ (CH_3) chemical shift positions are highly sensitive to L and Q^- identity and occur over a wide range (Table 2).[4a,39,40]

Note that the observed **4***/ZRS400 δ(Zr−CH_3) is located at the low-field extreme of values reported for $Cp'Zr(CH_3)_2^+$ species, suggesting highly electrophilic
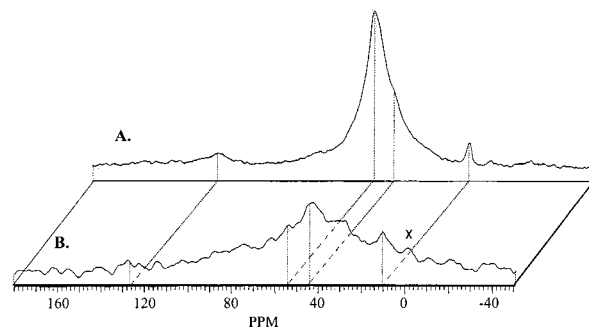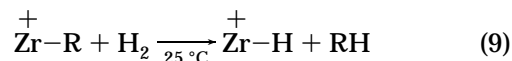

Figure 4. ^{13}C CPMAS NMR spectra of (A) $Cp'Zr(^{13}CH_3)_3$-(**4***)/ZRS400 (10 600 scans, repetition time = 2.2 s, contact time = 0.6 ms, spinning speed = 5.2 kHz) and (B) **4***/ZRS400 after benzene hydrogenation (6020 scans, repetition time = 2.2 s, contact time = 0.8 ms, spinning speed = 6.3 kHz).

Table 2. Solution and Solid-State ^{13}C NMR δ (Zr−CH_3) Data of Cationic Species $[Cp'Zr(CH_3)_2]^+Q^-$ and $[Cp'Zr(CH_3)_2(L)]^+Q^-$

complex	δ (Zr−CH_3)	reference
$[Cp'Zr(CH_3)_2]^+MePBB^-$ [a]	45.07[b]	4a
$[Cp'Zr(CH_3)_2(\eta^6$-PhMe$)]^+MeB(C_6F_5)_3^-$	45.5[b]	39a
$[Cp'Zr(CH_3)_2(\eta^6$-1,3,5-$C_6H_3Me_3)]^+$ $MeB(C_6F_5)_3^-$	40.7[b]	39a
$[Cp'Zr(CH_3)_2(THF)_2]^+BPh_4^-$	50.5[b]	39b
$[Cp'Zr(CH_3)_2(THF)(dmpe)]^+BPh_4^-$	34.6[b]	39b
$Cp'Zr(CH_3)_3/Al_2O_3^c$	42[d]	40
$Cp'Zr(CH_3)_3/ZRS400$	53.0[d]	this work

[a] PBB = tris(2,2′,2″-nonafluorobiphenyl)borane. [b] Measured in solution. [c] Al_2O_3 calcination temp = 500 °C. [d] Measured by solid-state CPMAS NMR.

character. Figure 4B shows the spectrum of **4***/ZRS400 after use in arene hydrogenation (vide infra) at 25 °C, 1.0 atm H_2. Note that while the Zr−CH_3 resonance of the μ-oxo species at δ 44 and the Cp−CH_3 signal at δ 9.0 are essentially unperturbed, the "cationic" Zr−CH_3^+ signal at δ 53.0 is significantly diminished, which likely results from M−CH_3 bond hydrogenolysis (eq 9, vide infra). This hydrogenolytic diminution of the "cationic"

$$\overset{+}{Zr}-R + H_2 \xrightarrow{25\,°C} \overset{+}{Zr}-H + RH \qquad (9)$$

Zr−CH_3^+ signal is in sharp contrast to the case of **1**/DA, where no major diminution of the M−$^{13}CH_3^+$ signal is observed, even after heating for several hours at 100 °C under H_2.[6e,i] This difference is in excellent agreement with the high percentage of **4**/ZRS400 catalytically active sites (∼68%) compared to those of **1**/DA (≲10%) inferred from poisoning experiments (vide infra). The prominent $Cp'Zr(^{13}CH_3)_2O-$ feature at δ 44 remaining unperturbed after hydrogenolysis/hydrogenation experi-

(37) (a) Dahmen, K.-H.; Marks, T. J. Unpublished results. (b) Jordan, R. F.; Dasher, W. E.; Echols, S. F. *J. Am. Chem. Soc.* **1986**, *108*, 1718−1719.

(38) Antiñolo, A.; Carrillo-Hermosilla, F.; Corrochano, A.; Fernández-Baeza, J.; Lara-Sanchez, A.; Ribeiro, M. R.; Lanfranchi, M.; Otero, A.; Pellinghelli, M. A.; Portela, M. F.; Santos, J. V. *Organometallics* **2000**, *19*, 2837−2843.

(39) (a) Gillis, D. J.; Tudoret, M.-J.; Baird, M. C. *J. Am. Chem. Soc.* **1993**, *115*, 2543−2545. (b) Crowther, D. J.; Jordan, R. F.; Baenzinger, N. C.; Verma, A. *Organometallics* **1990**, *9*, 2574−2580.

(40) Jezequel, M.; Dufaud, V.; Ruiz-Garcia, M. J.; Carrillo-Hermosilla, F.; Neugebauer, U.; Niccolai, G. P.; Lefebvre, F.; Bayard, F.; Corker, J.; Fiddy, S.; Evans, J.; Broyer, J.-P.; Malinge, J.; Basset, J.-M. *J. Am. Chem. Soc.* **2001**, *123*, 3520−3540.
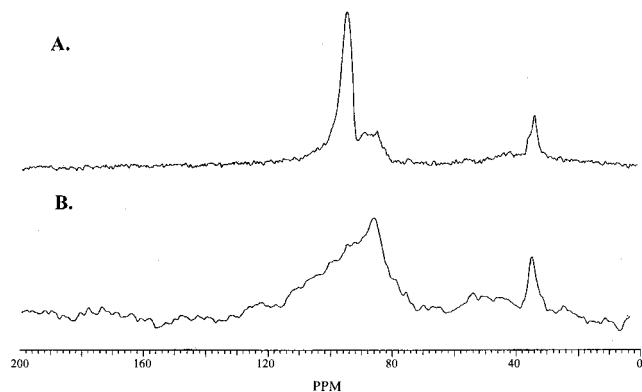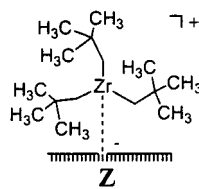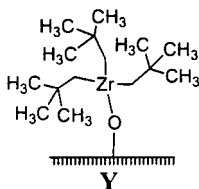
Figure 5. ^{13}C CPMAS NMR spectra of (A) $Zr(^{13}CH_2{}^{t}Bu)_4$ (**6***)/PDS (10030 scans, repetition time = 4 s, contact time = 1.0 ms, spinning speed = 7.4 kHz) and (B) **6***/ZRS400 (7500 scans, repetition time = 4 s, contact time = 1.0 ms, spinning speed = 5.9 kHz).

ments supports the lower surface μ-oxo adsorbate reactivity, in accord with the solution chemistry of the analogous and clearly nonelectrophilic f-element Cp′₂-Th(CH₃)OR analogues.[31,41]

The adsorption chemistry of labeled complex **6***, Zr-($^{13}CH_2{}^{t}Bu)_4$, on PDS and ZRS400 was examined to probe the fate of alkyl ligands originally coordinated to a homoleptic Zr hydrocarbyl, and the resulting adsorbate structure (note that **6**/PDS has been reported to exhibit unique catalytic activity[42]). The α-methylene carbon resonance of complex **6** at δ 103.0 in C_6D_6 is readily identified by ^{13}C labeling. The ^{13}C CPMAS spectrum of **6***/PDS exhibits three bands (Figure 5A). The most prominent feature at δ 94.7 is assigned to a μ-oxo species (${}^{t}Bu^{13}CH_2)_3ZrO-$; e.g., structure **Y**), by analogy with δ 100.1 for the homogeneous analogue (${}^{t}Bu^{13}CH_2)_3ZrO-[4-Me2,6-4({}^{t}Bu)_2C_6H_2]$.[43] Although the weak resonance at δ 87 cannot be rigorously assigned, a (${}^{t}Bu^{13}CH_2)_2Zr(O^-)_2$ structure is consistent with the methylene group assignment deduced from interrupted decoupling experiments (vide infra) and the observation that the chemical shift is further upfield than for μ-oxo species such as (${}^{t}Bu^{13}CH_2)_3ZrO-$. An identical structure chemisorbed on the silica and partially dehydroxylated alumina has been previously suggested.[44] The other resonance at δ 33.5 can be straightforwardly assigned to a neopentyl C_γ group, compared to δ 35.3 for the analogous carbon of complex **6*** in solution. Nonlabeled complex **6** chemisorbed on PDS was reported to exhibit only this band.[44a] The protonolytic reaction pathway of homoleptic complex **6*** with partially dehydroxylated silica thus parallels that of model compounds **1***/PDS and **2***/PDS as well as organozirconium compounds **3*** and **4*** (vide supra).

The solid-state ^{13}C CPMAS NMR spectrum of **6***/ZRS400 is shown in Figure 5B. At least three labeled

(41) Mintz, E. A.; Moloy, K. G.; Marks, T. J.; Day, V. W. *J. Am. Chem. Soc.* **1982**, *104*, 4692–4695.

methylene signals are observed in the low-field region (>δ 80), and a single band in the high-field region (~δ 34), the latter of which is again straightforwardly assigned to a neopentyl C_γ resonance. By analogy with the spectrum of **6***/PDS, the two features at δ 95 and 86 are assignable to μ-oxo (e.g., **Y**) and di-μ-oxo species from previous arguments. Additionally, the relatively broad band centered at ca. δ 105 can be reasonably assigned to a cationic $[Zr(^{13}CH_2{}^{t}Bu)_3]^+$ species on the basis of the low-field $\delta(M-^{13}CH_2R)$ character and catalytic activity (vide infra; e.g., **Z**). Again, there is no evidence of significant alkide transfer to surface Lewis acid sites (cf., the ^{13}C CPMAS spectrum of ${}^{t}Bu^{13}CH_2Li/$ DA, which exhibits an $Al_{surface}-^{13}CH_2{}^{t}Bu^-$ resonance at δ 29).[45] An interrupted decoupling spectrum of **6***/ ZRS400 was obtained with a 125 μs delay inserted before data acquisition. For this delay time, dipolar dephasing for the significantly rigid methine and methylene $C-H$ groups is sufficient to induce signal diminution and eventual disappearance, and even methyl resonances, which have greater rotational freedom, are significantly diminished in intensity.[46] With careful referencing efforts, measured chemical shifts were reproducible to within $\pm\delta$ 0.1. All bands in the low-field region (>δ 80) disappear, in agreement with the above α-methylene assignment. The broad multiband envelope maximum at δ 34.7 is shifted slightly to δ 32.3 but is not suppressed, which supports an assignment as a nonprotonated carbon site, e.g., C_β.

In summary, sulfated zirconia again undergoes reaction with zirconium hydrocarbyl complexes **3***, **4***, and **6*** to afford "cation-like" surface species, and the transfer of methide/alkide groups to the oxide surface is below the detection limits in all cases, in marked contrast to chemisorption processes on DA or $MgCl_2$ (eq 1).[6c,e,g,i] In all cases examined, the hydrocarbyl groups are instead evolved as the corresponding hydrocarbons.

II. Supported Organozirconium Complex Catalysis. (A) Activity Measurements and Kinetics of 1-Hexene/Arene Hydrogenation. 1-Hexene and arene hydrogenation reactions using the supported organozirconium catalysts were studied in two different types of reactor (see Experimental Section for details). Reactor A employed a Barocel differential electronic manometer between two glass gas ballasts in an isothermal bath (25.0 ± 0.1 °C). It was equipped with a high-speed vortex agitator and was capable of measuring hydrogen uptake with high precision under ambient conditions (20–30 °C; pressure, 1.0 atm H_2). Two burets are attached to the reaction chamber, which affords experimental conveniences such as in situ titration or poisoning experiments. Reactor A was used for α-olefin

(42) (a) Quignard, F.; Graziani, O.; Choplin, A. *Appl. Catal. A.: General* **1999**, *182*, 29–40. (b) Niccolai, G. P.; Basset, J.-M. *Appl. Catal. A.: General* **1996**, *146*, 145–156. (c) Corker, J.; Lefebvre, F.; Lécuyer, C.; Dufaud, V.; Quignard, F.; Choplin, A.; Evans, J.; Basset, J.-M. *Science* **1996**, *271*, 966–969.

(43) Miller, J. B.; Schwartz, J.; Carroll, K. M. *Organometallics* **1993**, *12*, 4204–4206.

(44) (a) Quignard, F.; Lecuyer, C.; Bougault, C.; Lefebvre, F.; Choplin, D. O.; Basset, J.-M. *Inorg. Chem.* **1992**, *31*, 928–930. (b) Miller, J. B.; Schwartz, J. *Inorg. Chem.* **1990**, *29*, 4579–4581.

(45) H. Ahn; Marks, T. J. Unpublished results.

(46) (a) Witt, J.; Fenzke, D.; Hoffmann, W. D. *Appl. Magn. Reson.* **1992**, *3* (1), 151–163. (b) Newman, R. H. *J. Magn. Reson.* **1992**, *96* (2), 370–375. (c) Alemany, L. B.; Grant, D. M.; Alger, T. D.; Pugmire, R. J. *J. Am. Chem. Soc.* **1983**, *105*, 6697–6704. (d) Opella, S. J.; Frey, M. H.; Cross, T. A. *J. Am. Chem. Soc.* **1979**, *101*, 5854–5856.
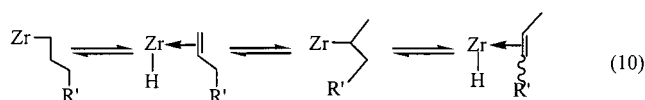
Table 3. Olefin/Arene Hydrogenation Catalyzed by Organozirconium Complexes Chemisorbed on Zirconia (ZR) and Various Sulfated Zirconias (ZRSx)[a]

entry	complex	reactor	temp, °C	P_{H_2}, psi	solid acid support	substrate	N_t,[b] h^{-1}
1	Cp$_2$Zr(CH$_3$)$_2$ (**3**)	A	25.0	14.7	ZR	1-hexene	$\sim$0[c]
2	**3**	A	25.0	14.7	ZRS300	1-hexene	32[d]
3	**3**	A	25.0	14.7	ZRS400	1-hexene	35[d]
4	**3**	A	25.0	14.7	ZRS740	1-hexene	7[d]
5	Cp′Zr(CH$_3$)$_3$ (**4**)	A	25.0	14.7	ZRS400	1-hexene	2840
6	**4**	A	25.0	14.7	ZRS400	benzene	970
7	r(CH$_2$TMS)$_4$ (**5**)	B	90.0	180	ZRS400	benzene	1060
8	Zr(CH$_2$tBu)$_4$ (**6**)	B	90.0	180	ZRS400	benzene	785
9	Zr(CH$_2$Ph)$_4$ (**7**)	B	90.0	180	ZRS400	benzene	420

[a] In a typical experiment, 50 mg of catalyst ([Zr] = 7.4 × 10^{-3} mmol) was agitated in 0.020 mL of 1-hexene (1.6 × 10^{-1} mmol) + 1.0 mL of octane solution (entries 1−5) or 1.0 mL of neat arene (entries 6−8) at a speed of 2000 rpm. [b] Turnover frequency values were measured while the pressure drop in system was <1%. All H$_2$ uptake results are corrected for substrate vapor pressure. [c] In NMR scale experiments, hexane was detected by ^{1}H NMR after 2 days at 70 °C. [d] Double bond migration was observed. See text.

hydrogenation activity measurements (Table 3, entries 1−5), sensitive hydrogen uptake measurements on highly active catalysts under ambient conditions (entries 5, 6), and poisoning experiments (vide infra). Reactor B was employed for accurate monitoring of hydrogen uptake for catalysts exhibiting moderate activity (Table 3, entries 7−9) and kinetic experiments under various conditions (30−200 °C; 1.0−20 atm H$_2$ pressure). Turnover frequency (N_t) is defined as moles of substrate converted per moles Zr per time.

(i) 1-Hexene Hydrogenation. A series of experiments with 1-hexene established rapid H$_2$ gas uptake at 25 °C, 14.7 psi H$_2$ in reactor A. Control experiments established that kinetic measurements at stirring velocities of the slurries greater than $\sim$1500 rpm are not influenced by H$_2$ mass transfer effects (Figure 6). The relative 1-hexene hydrogenation activities fall in the order **4**/ZRS400 ≫ **3**/ZRS400 ≥ **3**/ZRS300 > **3**/ZRS720 ≫ **3**/ZR $\sim$ 0, as demonstrated in Table 3 (entries 1−5) and Figure 7. Kinetic measurements of 1-hexene hydrogenation mediated by **3**/ZRS400 and **3**/ZRS720 exhibit what initially appeared to be a rather complex time dependence. This was found to arise from two unexpected side reactions: 1-hexene double bond migration and 1-hexene oligomerization. The double bond migration process (eq 10) is dominant for **3**/ZRSx, which exhibits relatively low hydrogenation activity (not surprisingly, some classes of supported zirconium hydrides such as ZrH/SiO$_2$ catalyze olefin isomerization more rapidly than hydrogenation[47h]). GC/MSD analysis at

$$Zr\!-\!\!\diagup\!\!\diagdown^{R'} \;\rightleftharpoons\; Zr\!\leftarrow\!\|\atop H \;\diagdown_{R'} \;\rightleftharpoons\; Zr\!-\!\!\diagup\!\!\diagdown_{R'} \;\rightleftharpoons\; Zr\!\leftarrow\!\|\atop H \;\diagdown_{R'} \tag{10}$$

different stages of conversion indicates the appearance and growth of *trans*- and *cis*-2-hexene in the reaction mixture. For **3**/ZRS400, $\sim$14% conversion to 2-hexene (*trans* + *cis*) is observed after 70% substrate hydrogenation, while for **3**/ZRS720, $\sim$35% conversion to 2-hexene (*trans* + *cis*) occurs after 70% substrate hydrogenation. Relative olefin hydrogenation activities with respect to different olefins are not expected to be identical.[48] Also, it is conceivable that 1-hexene oligomerization may be
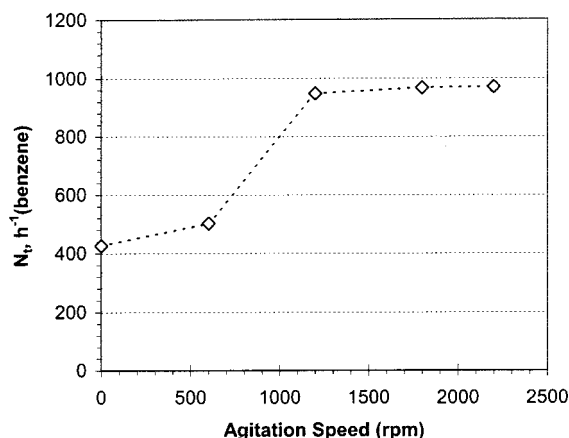
Figure 7. (A) Time dependence of H$_2$ consumption in reactor **A** for Cp$_2$Zr(CH$_3$)$_2$ (**3**)/ZRS400-, **3**/ZRS300-, and **3**/ZRS740-catalyzed hexene hydrogenation. (B) Time dependence of H$_2$ consumption in reactor **A** for Cp′Zr(CH$_3$)$_3$ (**4**)/ZRS400-catalyzed hexene hydrogenation.

Figure 6. Data establishing hydrogenation mass transfer rate limits for Cp′Zr(CH$_3$)$_3$ (**4**)/ZRS400-catalyzed benzene hydrogenation using reactor A.
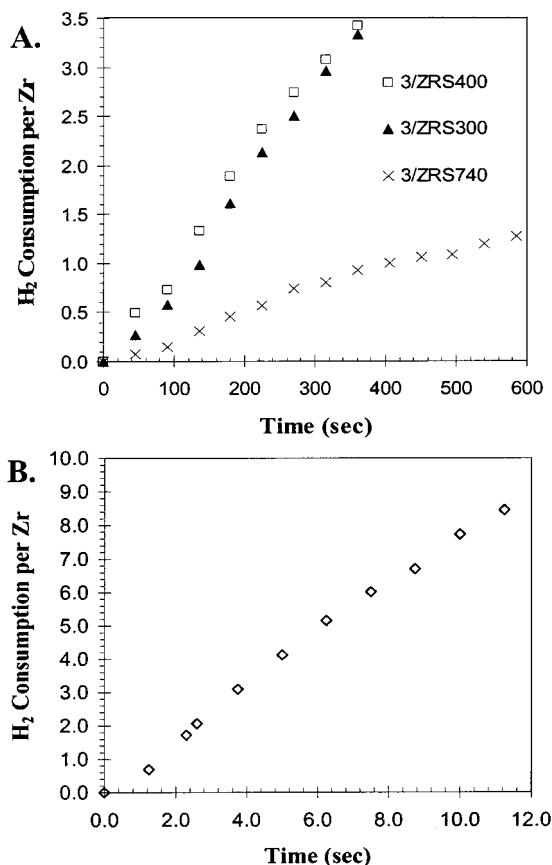
Table 4. Arene Products and Hydrogenation Activity Data for Cp′Zr(CH₃)₃ (4)/ZRS400 at 25.0 °C, 14.7 psi H₂ (1.0 atm)[a]

substrate	product	N_t, × 10⁻¹, s⁻¹ [b]
C₆H₆	C₆H₁₂	4.15[c]
C₆D₆	C₆H₆D₆	4.10[c]
CH₃C₆H₅	CH₃C₆H₁₁	0.060[c]
1,4-(CH₃)₂C₆H₄	−	−

[a] P_{H_2} = 1.0 atm, temp = 25 °C. [b] Turnover frequency normalized for the number of active [Zr]. [c] Turnover frequency is independent of conversion.

mediated cationically via the residual acid sites of the sulfated zirconia, as evidenced by a blank experiment with pure sulfated zirconia.[49] The oligomers formed entrain the catalyst, and diminishing activities are observed as the reaction proceeds. Both substrate isomerization and oligomerization significantly complicate the precise hydrogenation kinetic measurements. Therefore, the N_t values in Table 3 are reported for the initial ≤20% conversion, during which time 1-hexene isomerization or oligomerization is minor. Note that mono-Cp complex **4** supported on sulfated zirconia exhibits significantly enhanced olefin hydrogenation activity, an observation that appears to be steric in origin.

(ii) Arene Hydrogenation. From the studies of ZRSx-mediated 1-hexene hydrogenation, it was found that ZRS400 yields the highest catalytic activity among the supports investigated. To investigate steric factors affecting catalytic pathways, a series of more "open" non-Cp precatalysts, **5**, **6**, and **7**, were surveyed for arene hydrogenation activity. The measurements were performed with **4**/ZRS400 (Table 3, entry 6 and Table 4) in reactor A and with **5**/, **6**/, and **7**/ZRS400 (Table 3, entries 7−9) in reactor B, respectively. Both reactors were under vigorously stirred, non-mass transfer-limited conditions. The relative activity for benzene hydrogenation was discovered to be **4**/ZRS400 ≫ **5**/ZRS400 > **6**/ZRS400 > **7**/ZRS400. In Table 5, the present rate data are compared to those of catalyst-immobilized[6b,47] or conventional heterogeneous arene hydrogenation catalysts.[50,51] Strikingly, the benzene hydrogenation activity of **4**/ZRS400 rivals or exceeds those of the most active heterogeneous arene hydrogenation catalysts known. GC/MSD and ¹H NMR analysis at various conversion stages indicates that any partially hydrogenated products such as cyclohexadiene or cyclohexene are present

Table 5. Kinetic Data for Catalytic Benzene Hydrogenation of Benzene by the Indicated Heterogeneous Catalysts

catalyst	temp, °C	pressure, psi	N_t,[a] h⁻¹	reference
PtCl₂(CH₃CN)₂ + BF₃·H₂O/ zeolite	75	800	1330	47h
Rh/H-Erionite	80	100	1728	50d
Zr(hydride)/SiO₂	90	20	83	47i
0.5% Rh/SrTiO₃	30	14	458	45d
(η⁵-Me₅C₅)Th(CH₂C₆H₅)₃/ Al₂O₃	90	190	765	6b
Th(η³-C₃H₅)₄/Al₂O₃	90	190	1970	6b
0.89% NiR/Y zeolite[b]	80	90	1200	47f
RhCl(CO)₂R/Pd-SiO₂[c]	40	14	60	47c
(η⁵-Me₅C₅)Zr(CH₃)₃ (**4**)/ ZRS400	25	14	970	this work
Zr(CH₂TMS)₄(**5**)/ZRS400	90	180	1060	this work

[a] Measured turnover frequency under conditions quoted. [b] R = 2-(3-triethoxysilylpropylaminocarbonyl)pyrrolidine. [c] R = [Et₂N-(CH₂)₃Si(OCH₃)₃].

below the detection limits (≤10⁻⁴%). This feature can be contrasted with the behavior of many conventional late transition metal heterogeneous arene hydrogenation catalysts,[50] where free cyclohexene or cyclohexadiene is detected during conversion. However, the catalytic behavior of present catalysts resembles that of dehydroxylated alumina (DA)-supported organothorium catalysts,[6b] where cyclohexane is the only product at all stages of conversion.

Adsorbate **4**/ZRS400 also catalyzes the hydrogenation of methyl-substituted arenes (Table 4), and again, partially hydrogenated mixtures are not detected by GC/MSD. For a series of arenes, the relative rates fall in the order benzene ≫ toluene ≫ *p*-xylene ∼ 0. Interestingly, this general hydrogenation rate dependence on alkyl substituents generally holds for most conventional heterogeneous[50,5li] or organometal-immobilized arene hydrogenation catalysts[6b,47a−e] and is believed to arise from a combination of steric and electronic contributions. However, note that the arene hydrogenation activities of the present catalyst systems are far more sensitive to/selective for substituent effects than conventional heterogeneous catalyst systems (e.g, for **4**/ZRS400, N_t(benzene):N_t(toluene):N_t(*p*-xylene) = 1:0.014:0 at 273 K, 1.0 atm H₂, while for Ni/SiO₂,[51a] the ratio is 1:0.49:0.34 (*o*-xylene) at 393 K, 0.96 atm H₂, and for Th(allyl)₄/DA,[6b] the ratio is 1:0.60:0.21(*p*-xylene) at 363 K, 12.9 atm H₂). This marked substrate substituent selectivity suggests that the present Zr center is in a far more hindered environment than previously encoun-

(47) (a) Liu, A. M.; Hidajat, K.; Kawi, S. *J. Mol. Catal. A. Chem.* **2001**, *168*, 303−306. (b) Yang, H.; Gao, H.; Angelici, R. J. *Organometallics* **2000**, *19*, 622−629. (c) Gao, H.; Angelici, R. J. *New J. Chem.* **1999**, *6*, 633−640. (d) Gao, H.; Angelichi, R. J. *J. Am. Chem. Soc.* **1997**, *119*, 6937−6938. (e) Blum, J.; Rosenfeld, A.; Polak, N.; Israelson, O.; Schumann, H.; Avnir, D. *J. Mol. Catal. A: Chem.* **1996**, *106*, 217−223. (f) Corma, A.; Iglesias, M.; Sánchez, F. *Catal. Lett.* **1995**, *32*, 313−318. (g) Profilet, R. D.; Rothwell, A. P.; Rothwell, I. P. *J. Chem. Soc., Chem. Commun.* **1993**, 42−44. (h) Horváth, I. T. *Angew. Chem., Int. Ed. Engl.* **1991**, *30*, 1009−1011. (i) Yermakov, Y. I.; Ryndin, Y. A.; Alekseev, O. S.; Kochubey, D. I.; Schmachkov, V. A.; Gergert, N. I. *J. Mol. Catal.* **1989**, *49*, 121−132. (j) Schwartz, J.; Ward, M. D. *J. Mol. Catal.* **1980**, *8*, 465−469.

(48) As a function of olefin, relative Cp′₂Th(CH₃)₂/DA catalytic hydrogenation activities are *cis*-2-butene > *trans*-2-butene > propylene > isobutylene.[6f]

(49) There are several typical examples of cationic olefin polymerization mediated by solid acids including sulfated zirconia. See: (a) Sarin, R.; Tuli, D. K.; Sinharay, S.; Rai, M. M.; Ghosh, S.; Bhatnagar, A. K. *Prepr.-Am. Chem. Soc., Div. Pet. Chem.* **1996**, *41* (3), 625−627. (b) Sanyo Chemical Industries, Ltd., Jpn. Pat. 8 226 626, 1982. (c) Marquis, E. T.; Watts, L. W.; Braker, W. H.; Aden, J. W. Belgian Pat. 891 533, 1982.

(50) (a) Rahman, M. V.; Vannice, M. A. *J. Catal.* **1991**, 127, 251. (b) Siegel, S. In *Comprehensive Organic Synthesis*; Trost, B. M., Fleming, I., Eds.; Pergamon Press: Oxford, 1991; Vol. 8, Chapter 31. (c) Timmer, K.; Thewissen, D. H. M. W.; Meinema, H. A.; Bulten, E. J. *Recl. Travl. Chim. Pays-Bays* **1990**, *109*, 87−92. (d) Pajonk, G. M.; Teichner, S. J. In *Catalytic Hydrogenation*; Cerverneý, L., Ed.; Elsevier: Amsterdam, 1986; Chapter 8. (e) Bartók, M. *Stereochemistry of Heterogeneous Metal Catalysis*; Wiley: New York, 1985; Chapter V. (f) Rylander, P. N. *Catalytic Hydrogenation in Organic Synthesis*; Academic Press: New York, 1979; Chapter 11. (g) Leitz, G.; Volter, J. In *Mechanism of Hydrocarbon Reactions*; Elsevier: Amsterdam, 1975; pp 151−162.

(51) (a) Keane, M. A.; Patterson, P. M. *J. Chem. Soc., Faraday Trans.* **1996**, *92*, 1413−1420. (b) Coughlan, B.; Keane, M. A. *Zeolites* **1991**, *11*, 12−17. (c) Mirodatos, C.; Dalmon, J. A.; Martin, G. A. *J. Catal.* **1987**, *105* (2), 405−415. (d) Prasad, K. H. V.; Prasad, K. B. S.; Mallikarjunan, M. M.; Vaidyeswaren, R. *J. Catal.* **1983**, *84*, 65−73. (e) Suzuki, M.; Tsutsumi, K.; Takahashi, H. *Zeolites* **1982**, *2*, 51−58. (f) Taylor, W. F.; Yates, D. J. C.; Sinfelt, J. H. *J. Phys. Chem.* **1964**, *68*, 2962−2966. (g) Canjar, L. N.; Manning, F. S. *J. Appl. Chem.* **1962**, *12*, 73−74.
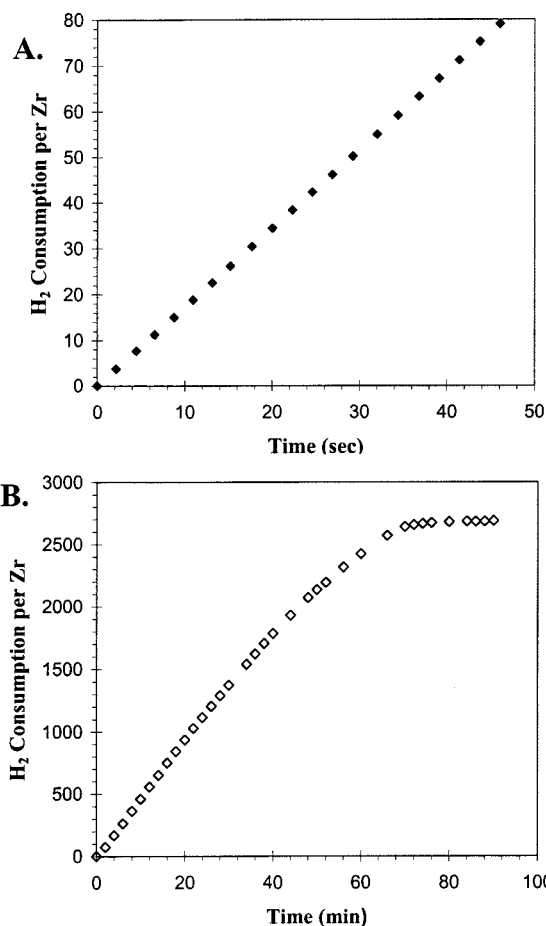
Figure 8. (A) Time dependence of H_2 consumption per Zr in the reactor **A** for the $Cp'Zr(CH_3)_3$(**4**)/ZRS400-catalyzed benzene hydrogenation. (B) H_2 pressure in reactor **B** in the $Zr(CH_2TMS)_4$ (**5**)/ZRS400-catalyzed benzene hydrogenation.
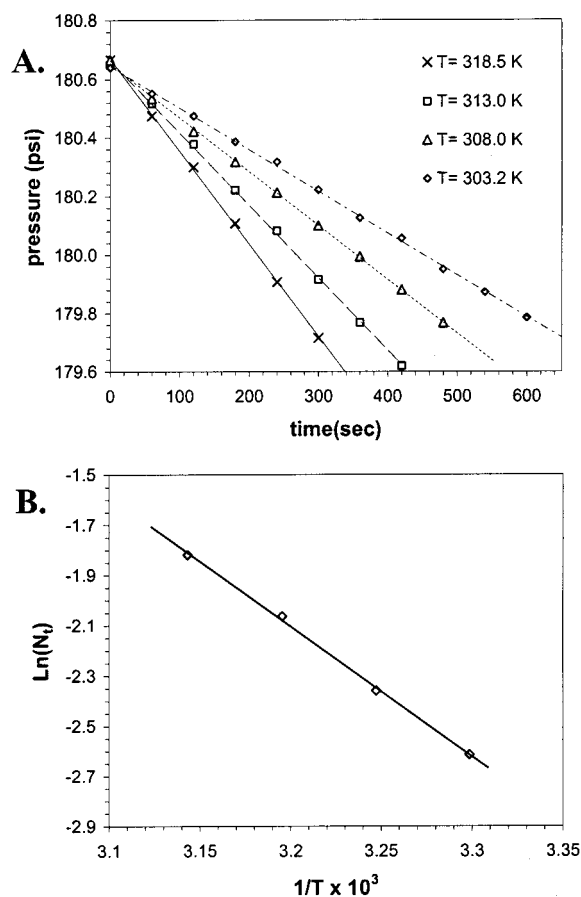

Figure 9. (A) Temperature dependence of H_2 consumption per Zr in the reactor **A** for the $Zr(CH_2TMS)_4$(**6**)/ZRS400-catalyzed benzene hydrogenation, and (B) Arrhenius plot for benzene hydrogenation catalyzed by **6**/ZRS400.
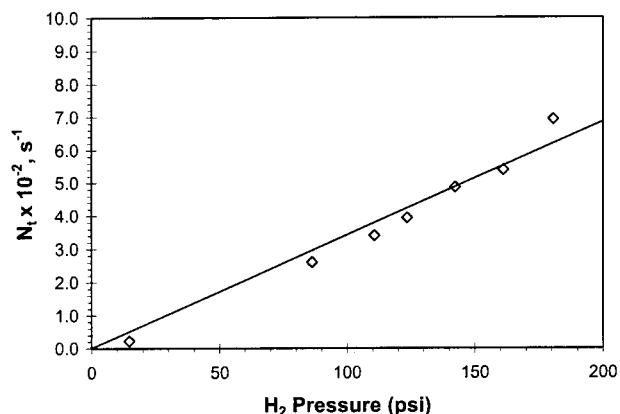

Figure 10. H_2 pressure dependence of the observed turnover frequency for **6**/ZRS400-catalyzed benzene hydrogenation.

tered, presumably originating from intrinsic surface steric hindrance and/or the presence of coordinated $O_{surface}$ in the metal coordination sphere. However, the difference in ligand system electronic factors, mono-Cp vs non-Cp should also be stressed in rationalizing the diverse catalytic activities.

A kinetic study of benzene hydrogenation by **6**/ZRS400 was also conducted over a range of temperatures (303.2−318.5 K) at 180.65 psi H_2. The data and the resulting Arrhenius plot are shown in Figure 9. The derived activation energy from a least-squares analysis is $E_a = 10.3 \pm 0.8$ kcal/mol. The rate measurements of benzene hydrogenation show that hydrogenation rates of catalysts **4**/ZRS400, **5**/ZRS400, **6**/ZRS400, and **7**/ZRS400 are all zero-order in substrate concentration (time-independent N_t) over a broad benzene concentration range (Figure 8). Measurements of the rates of benzene hydrogenation by **6**/ZRS400 at various H_2 pressure also establish first-order kinetic dependence on hydrogen pressure (Figure 10).

(B) Benzene Hydrogenation Regiochemistry. GC/MSD and NMR analysis of the reduction product of C_6D_6 with H_2 reveals that $C_6H_6D_6$ is the exclusive product and that there is no evidence of C−H/C−D exchange in the reaction mixture. ^{13}C and ^{13}C{^{1}H} 125.6 MHz NMR spectra of the $C_6H_6D_6$ product at room temperature suggest the presence of at least two

regioisomers (Figure 11A) and that every ring carbon has a single H and a single D substituent (Figure 11B). In previous supported organothorium work,[6b] the $C_6H_6D_6$ ^{13}C NMR spectrum was assigned by correlating theoretically generated spectra with the low-temperature (−100 °C) ^{13}C NMR spectrum,[52] which is in good agreement with the 1:3 mixture spectrum of the all-*cis* (denoted $\alpha\alpha\alpha$) and the *cis, cis, trans, cis, trans* (denoted $\alpha\alpha\beta$) regioisotopomers. The present assignments were also correlated with the ^{13}C NMR spectra of $C_6H_6D_6$ produced by Th(allyl)$_4$/DA, which exhibits two sets of triplets (1.0:2.9).[6b] In the present investigation, the ^{13}C
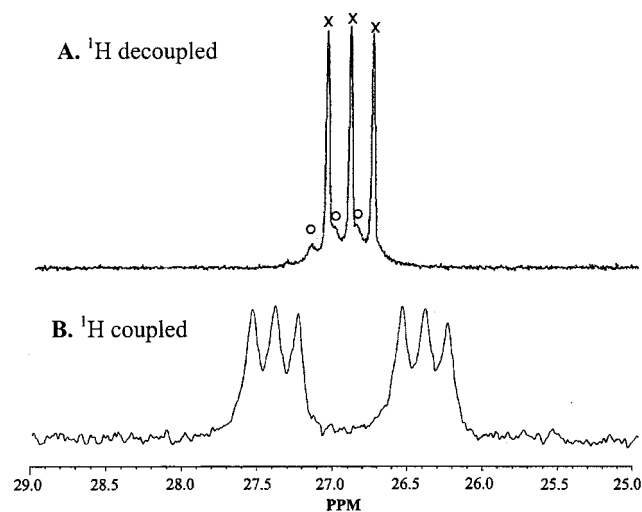
Figure 11. (A) $^{13}C\{^1H\}$ spectrum of the cyclohexane product of $Cp'Zr(^{13}CH_3)_3$(**4**)/ZRS400-meditated hydrogenation of C_6D_6. The Xs and Os denote the different isotopomers. (B) ^1H coupled ^{13}C spectrum of the product in part A.

NMR pattern of the $C_6H_6D_6$ product is indistinguishable from that of the previously reported one except for the relative intensities of regioisotopomers: two sets of $^{13}C-$ ^2H coupled triplets indicated by $\bigcirc$ (δ 26.93, $^1J_{C-D}$ = 19 Hz) and $\times$ (δ 27.02, $^1J_{C-D}$ = 19 Hz). The two triplets are therefore straightforwardly assigned to the all-*cis* ($\alpha\alpha\alpha$; as designated by $\bigcirc$ in Figure 11A) and to the *cis, cis, trans, cis, trans* regioisotopomers ($\alpha\alpha\beta$, designated by $\times$ in Figure 11A) from the analogous ^{13}C NMR spectra. That is, individual H_2 units are delivered in a pairwise fashion to a single face of the arene skeleton. Integration of the two triplets indicates the regioisotopomers are formed in the ratio of 1.0 ($\alpha\alpha\alpha$):3.1 ($\alpha\alpha\beta$).

$\alpha\alpha\alpha$ $\alpha\alpha\beta$
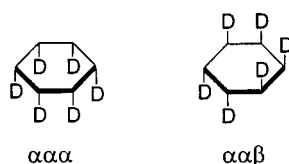
(C) Active Catalytic Site Assay. For conventional or molecular precursor-based heterogeneous catalysts, it is not unusual that only a limited fraction of the surface sites is of catalytic significance.[6a−d,f,g,53] In previous studies, population measurements were conducted by poisoning with quantitative chemical probes and the catalytically significant populations of the supported organometallic catalysts assayed. Quantitative CO or protonolytic poisoning experiments reveal that $\sim$2−8% of $L_xAnR_{n'}$/DA and $\sim$35% of $Cp'_2An(CH_3)_2$/ $MgCl_2$ sites (An = Th, U) are catalytically important in olefin transformations.[6f] In the present study, D_2O was employed in poisoning experiments via the pathway

(52) Theoretical $^1H\{D\}$ spectra can be generated for static cyclohexane structures using literature chemical shift and $^1H-^1H$ coupling constant parameters. For reference, see: (a) Muetterties, E. L.; Rakowski, M. C.; Hirsekorn, F. J.; Larson, W. D.; Basus, V. J.; Anet, F. A. L. *J. Am. Chem. Soc.* **1975**, *97*, 1266−1267. (b) Haddon, V. R.; Jackman, L. M. *Org. Magn. Reson.* **1973**, *5*, 333−338. (c) Remijnse, J. D.; Vandeginste, B. G. M.; Webster, B. M. *Recl. Trav. Chim. Pays-Bas* **1973**, *92*, 804−808. (d) Barfield, M. *J. Am. Chem. Soc.* **1971**, *93*, 1066−1071 (e) Barfield, M. J.; Chakrabarti, B. *Chem. Rev.* **1969**, *69*, 757−778.
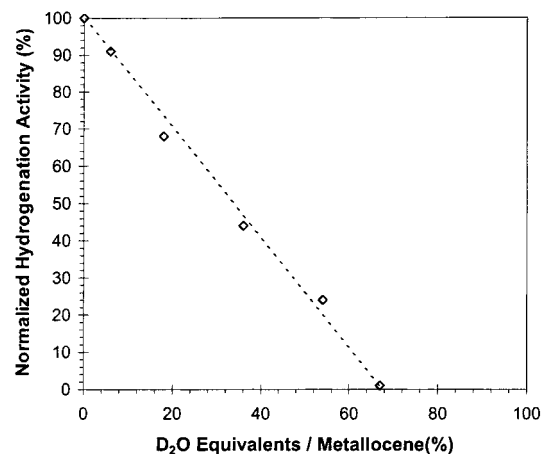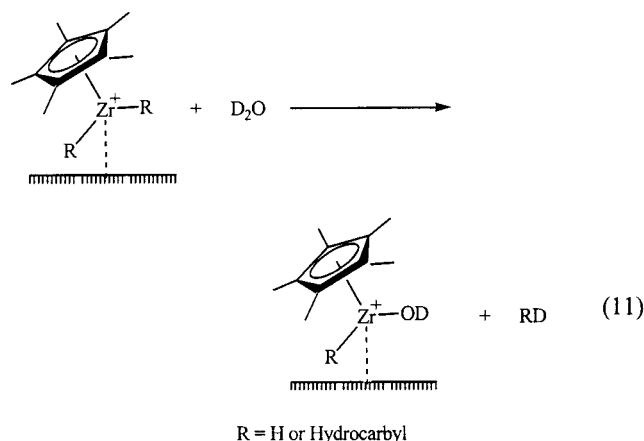

Figure 12. Poisoning experiment showing D_2O equivalents/ metallocene (%) dependence of normalized hydrogenation activity (%) in reactor **A** for **4**/ZRS400-catalyzed benzene hydrogenation.

suggested in eq 11, or a less likely variant in which

R = H or Hydrocarbyl

greater than one hydride/hydrocarbyl ligand is hydrolyzed to form a $Zr-(OH)_n$ species (n = 2, 3). This protonolysis pathway is verified by exclusive identification of Np-D after treating **7**/ZRS400 with D_2O. Active site counting experiments for benzene hydrogenation by the **4**/ZRS400 catalyst were performed with reactor **A**. Measured, substoichiometric aliquots of degassed D_2O in benzene were introduced from the attached buret, and catalytic activity was assessed for 10 min after each aliquot was added. The kinetics remain zero-order in benzene for each measurement. Figure 12 correlates the normalized catalytic activity change with equivalents of poison added. From these results, it can be concluded that (1) a maximum of $\sim$68% of complex **4** on ZRS400 is of catalytic significance and (2) the "linear" diminution of hydrogenation activity suggests that all active sites are kinetically identical in reaction with the D_2O poison.

(D) Polymerization of Olefins by Supported Organozirconium Complexes. (i) Homopolymerization of Ethylene. High-pressure ethylene homopolymerization experiments were performed with measured quantities of the present supported catalysts (4.1−4.8 μmol of Zr) at 150 psi C_2H_4 at 60 °C for 0.75− 2.0 min in 5.0 mL of toluene with rapid stirring ($>$1500 rpm) to minimize olefin mass transport effects (Table 6). Compared to conventional heterogeneous supported

Table 6. Summary of Ethylene Homopolymerization by Organozirconium Complexes Supported on Sulfated Zirconia (ZRSx)[a]

entry	catalyst	$[Zr]$ (μmol)	reaction time (s)	PE (g)	activity[b] $\times 10^6$	M_w[c] $\times 10^3$	M_w/M_n	T_m (°C)
1	Cp′Zr(CH₃)₃ (**4**)/ZRS400	4.3	120	0.110	0.77	d		
2	Zr(CH₂TMS)₄ (**5**)/ZRS400	4.5	60	0.137	1.8	d		
3	Zr(CH₂tBu)₄ (**6**)/ZRS400	4.8	60	0.098	1.2	1011[e]	1.6	133
4	Zr(CH₂Ph)₄ (**7**)/ZRS400	4.1	45	0.140	2.5	935[e]	1.4	134

[a] Carried out at 60 °C, 150 psi of ethylene, 5 mL of toluene. [b] Grams total polymer/mol Zr h. [c] GPC in 1,2,4-trichlorobenzene vs polystyrene standard. [d] Could not be measured due to low solubility. [e] Measured for a soluble fraction in 1,2,4-trichlorobenzene at 140 °C.

Table 7. Summary of Propylene Homopolymerization by Organozirconium Complexes Supported on Sulfated Zirconia (ZRSx)[a]

entry	catalyst	$[Zr]$ (μmol)	reaction time (min)	PP (mg)	activity[b] $\times 10^5$	M_w[c] $\times 10^3$	M_w/M_n	T_m (°C)	IR ratio[d]
1	Cp′Zr(CH₃)₃ (**4**)/ZRS400	4.3	5.0	0	0				
2	Zr(CH₂TMS)₄ (**5**)/ZRS400[e,f]	2.3	2.5	23	2.5	700[g]	2.8	149	1.69
3	Zr(CH₂tBu)₄ (**6**)/ZRS400[f,h]	4.8	5.0	67	1.7	420[g]	6.4	151	2.19
4	Zr(CH₂Ph)₄ (**7**)/ZRS400[f,i]	2.1	2.5	25	2.6	1070[g]	1.4	146	1.94

[a] Carried out at 25 °C, 7 mL of condensed neat propylene. [b] Grams total polymer/mol Zr h. [c] GPC in 1,2,4-trichlorobenzene vs polystyrene standard. [d] $A(974 \text{ cm}^{-1})/A(995 \text{ cm}^{-1})$. [e] Pentad composition (%): *mmmm* (19), *mmmr* (8.6), *rmmr* (4.8), *mmrr* (6.4), *mmrm* + *rmrm* (12.3), *rmrm* (7), *rrrr* (13.4), *mrrr* (14), *mrrm* (14). [f] Pentad compositions were measured in C₂D₂Cl₄ at 120 °C. [g] Measured for a soluble fraction in 1,2,4-trichlorobenzene at 140 °C. [h] Pentad composition (%): *mmmm* (25), *mmmr* (7.5), *rmmr* (2.4), *mmrr* (8.3), *mmrm* + *rmrm* (15.6), *rmrm* (5), *rrrr* (11), *mrrr* (16), *mrrm* (9). [i] Pentad composition (%): *mmmm* (24), *mmmr* (10), *rmmr* (5), *mmrr* (7), *mmrm* + *rmrm* (13.8), *rmrm* (7.2), *rrrr* (9.4), *mrrr* (7.9), *mrrm* (15.5).

catalysts,[3] the present catalysts exhibit moderate ethylene polymerization activities, as measured by quenching the polymerization reactions with methanol after a measured period, drying the product overnight, and weighing the resulting polymer. In contrast to olefin/arene hydrogenation, the ethylene polymerization activities of mono-Cp complex **4** and homoleptic complexes **5**, **6**, and **7** fall in a relatively narrow range, and activities follow the order **7** > **5** > **6** > **4**, a trend that approximately reflects coordinative saturation. Polyethylenes produced by the present catalysts have ultrahigh molecular weights (for the extracted fractions, $M_w \geq 10^6$), implicating a large propagation to chain transfer rate ratio. The formation of such high molecular weight polyethylene has been also reported for the ethylene polymerization mediated by related catalyst systems such as organozirconium adsorbates on alumina.[40]

(ii) Polymerization of Propylene. Table 7 summarizes results for high-pressure propylene polymerizations catalyzed by the present supported catalysts. Polymerization conditions such as the quantity of catalyst (2.1–4.8 μmol of Zr) and condensed propylene (7.0 mL) and polymerization time (2.5–5.0 min) were controlled in such a manner so as to achieve effective stirring (>1500 rpm) for the entire polymerization process. Catalysts **5**/ZRS400, **6**/ZRS400, and **7**/ZRS400 exhibit propylene polymerization activities comparable to those reported for other supported organozirconium polymerization catalysts,[3] and activities follow the same order as ethylene polymerizations: **7** > **5** > **6** ≫ **4** ∼ 0. Interestingly, catalyst **4**/ZRS400, which displays very high arene hydrogenation activity as well as moderate ethylene polymerization activity, exhibits marginal propylene polymerization activity (Table 7, entry 1). This characteristic is reminiscent of the aforementioned DA-supported organothorium systems in which the mono-Cp compound exhibits marginal activity, while homoleptic compound Th(η^3-allyl)₄/DA is moderately active for propylene polymerization.[6b] For the present catalysts, the resulting polymers are ultrahigh molecular

weight (Table 7, entries 2,4).[3,54] ¹³C NMR spectroscopic analyses for fractions soluble in C₂D₂Cl₄ at 120 °C (Table 6, entries 2–4) indicate that the resulting polypropylenes are *predominantly atactic*, with isotacticities ($P(mmmm)$): 19–25% vs atactic polypropylene $P(mmmm) = 6\%$) and synthiotacticities ($P(rrrr)$): 9.4–13.4% vs atactic polypropylene $P(rrrr) = 6\%$) slightly higher than observed/calculated for atactic polypropylene.[55] These atactic-rich structure populations are further supported by the IR absorbance ratios of the bands at 974 and 995 cm⁻¹; these are all in the range 1.69–2.19. Isotactic populations of hot-pressed films prepared from bulk polypropylenes produced by the present catalysts range from 33 to 46% based on published calibration curves.[56]

The high olefin/arene hydrogenation as well as α-olefin polymerization activities of the present catalysts confirm the results of the CPMAS studies which argue that the surface of sulfated zirconia affords relatively weakly coordinating chemisorption sites and activates organozirconium hydrocarbyl precatalysts to yield highly electrophilic "cation-like" species.

Discussion

I. The Chemisorption Process. Formation of Catalytically Active Sites. Sulfated zirconia has been a subject of intense research since the discovery of its remarkable activity in catalyzing hydrocarbon isomerizations under ambient conditions.[7,8] However, the origin of this unusual activity and the nature of active sites are still the subject of considerable debate. One of the goals of the present research is to define the intrinsic surface characteristics of sulfated zirconia using orga-

(53) (a) Kotrel, S.; Rosynek, M. P.; Lunsford, J. H. *J. Catal.* **1999**, *182* (1), 278–281. (b) Weddle, K. S.; Aiken, J. D., III; Finke, R. G. *J. Am. Chem. Soc.* **1998**, *120*, 5653–5666. (c) Fu, S.-L.; Rosynek, M. P.; Lunsford, J. H. *Langmuir* **1991**, *7*, 1179–1187, and references therein.
(54) Collette, J. W.; Tullock, C. W.; MacDonald, R. N.; Buck, W. H.; Su, A. C. L.; Harrell, J. R.; Mülhaupt, R.; Anderson, B. C. *Macromolecules* **1989**, *22*, 3851–3858.
(55) Ewen, J. A. *J. Am. Chem. Soc.* **1984**, *106*, 6355–6364.
(56) Luongo, J. P. *J. Appl. Polym. Sci.* **1960**, *3* (9), 302–309.

nozirconium complexes as "probe" molecules. After impregnating the complexes on the surface, the following active site models (structures **AA**, **AB**, **AC**, **AD**) can, in principle, be suggested. The present ^{13}C CPMAS NMR study readily excludes the significant participation by the structure **AB**, which was detected for metal complexes supported on DA, and **AD**, which was detected for the complexes supported on DS. Only two species, cationic structure **AA** as a major and μ-oxo adsorbate **AC** as a minor species, can be assigned.

AA   **AB**

AC   **AD**

(R^1, R^2, R^3, R^4 = Cp-ring or alkyl)
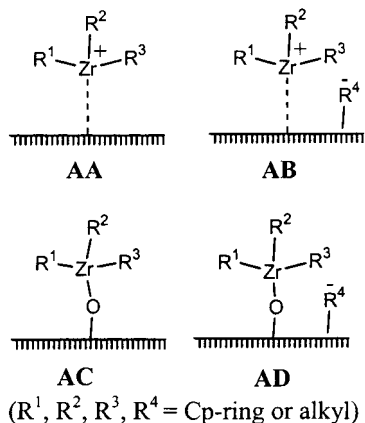
Interestingly, the present zirconium hydrocarbyls appear not to be activated on the Lewis acid sites (*cus*, coordinatively unsaturated sites) of sulfated zirconia, unlike on the surface of DA (structure **AB**). This observation supports the claimed weaker *Lewis acidity* of sulfated zirconia than that of DA.[25] As the ZRS activation temperature, T_a, increases, the number of Brønsted acid sites decreases and the number of Lewis acid sites increases.[26] Sulfated zirconia activated at 300–400 °C exhibits relatively constant Brønsted (~65%) and Lewis (~35%) site populations.[26] Sulfated zirconias activated at temperatures above 400 °C gradually lose Brønsted sites, which are primarily converted to Lewis acid sites. Therefore, the density of Brønsted acid sites can be correlated both with reported *n*-butane transformations and olefin hydrogenation rates in the present work, **3**/ZRS400 ≥ **3**/ZRS300 ≫ **3**/ZRS720. This supports a scenario in which the strong acid sites responsible for hydrocarbon transformations are also the ones that react with metal hydrocarbyls to afford cationic structures (via protonolysis) of type **AE**: an ion pair consisting of a cationic metallocene and the weak conjugate base of a strong Brønsted acid site (eq 12).[9a]

Equation 12 requires that the surface sulfate functionalities provide strong Brønsted acidity to form cationic species **AE** (evidenced by IR spectroscopy) and that the negative charge of the resulting conjugate base is so highly delocalized that coordination to the cationic zirconium center is minimal, unlike the case of conventional weak Brønsted acid (and strong conjugate base) surfaces such as ZR, PDS, or MgO. The ZRS oxo counteranion structure, characterized by extensive charge

delocalization, may explain the somewhat different features from potentially analogous chemistry in solution. Thus, oxo structure **AE** provides a more weakly coordinating environment than its seemingly homogeneous analogues such as $CF_3SO_3^-$, the conjugate acid ($H_o = -14.1$) of which affords catalytically marginal, covalently bound species.[57]

Since sulfated zirconia is known to also contain sites capable of oxidation, one could alternatively propose metal–hydrocarbyl bond activation via one-electron oxidation.[58] In an ^{1}H NMR experiment with complexes **3**, **6**, and **7** and sulfated zirconia, no alkyl radical coupling products, the plausible product of this radical mechanism (no radical disproportionation products are expected owing to lack of β-hydrogen atoms for R = CH$_3$, CH$_2$^{t}Bu, and CH$_2$Ph), were detected as might be expected from eq 13, pathway (i). Alternatively, if the

(13)
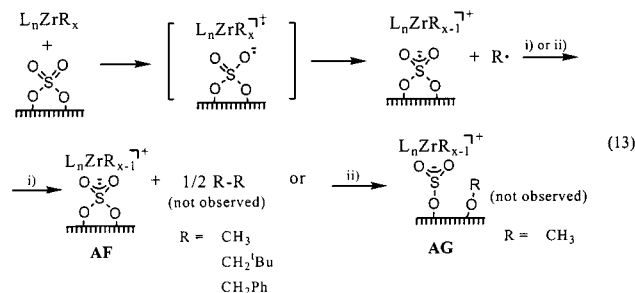
chemisorption follows pathway (ii) in eq 13, an intense resonance at ~δ 60 would be detected in the CPMAS spectra of **3***/ and **4***/ZRS400 (cf., in (^{t}Bu$_3$CO)$_2$Zr(OR)(OCH$_3$): R = CMe$_2$$\overline{\text{CHCH}_2}$O, δ (Zr–OCH$_3$) = 60.1).[59] However, no significant features of this type are detected in the ^{13}C CPMAS spectra of **3***/ and **4***/ZRS400. Therefore, it is concluded that one-electron oxidation is not a major route for group 4 metal hydrocarbyl activation.

It has been reported that homogeneous cationic zirconocene neopentyl complexes afford zirconium–methyl complexes and isobutylene via β-CH$_3$ elimination (eqs 14a,b) and that the equilibrium is dependent on steric crowding and electronic effects.[60] Thus, in eq 14a for Cp–R = C$_5$H$_3$(1,2-Me$_2$)[60a] and C$_5$Me$_5$,[60b] $k_1 \gg k_{-1}$ and for Cp–R = C$_5$H$_5$, $k_1 \geq k_{-1}$. In eq 14b, for Cp–R = C$_5$Me$_5$, β-CH$_3$ elimination is significant, while for Cp–R = C$_5$H$_5$, β-CH$_3$ elimination products are not detected.

For the case of **6**/ZRS400, the formation of free isobutene is below the ^{1}H NMR detection limits in slurry experiments. Alternatively, if the isobutene underwent cationic oligomerization/polymerization induced by residual strong Brønsted sites on the surface,[61] the ^{13}C CPMAS spectrum of **6***/ZRS400 should exhibit an intense resonance from the ^{13}C-enriched poly(isobutylene) methylene backbone at ~δ 60 in the ^{13}C CPMAS
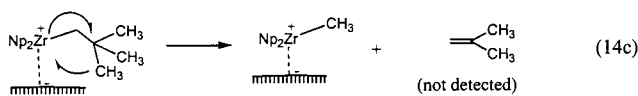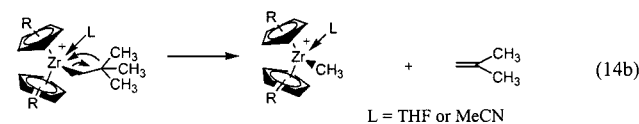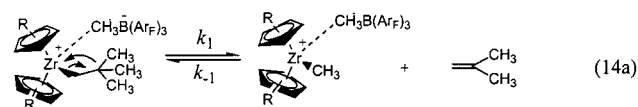
(57) Toscano, P. J.; Marks, T. J. Unpublished observations.
(58) (a) Borkowsky, S. L.; Baenzinger, N. C.; Jordan, R. F. *Organometallics* **1993**, *12*, 486–495. (b) Borkowsky, S. L.; Jordan, R. F.; Hinch, G. D. *Organometallics* **1991**, *10* (5), 1268–1274.
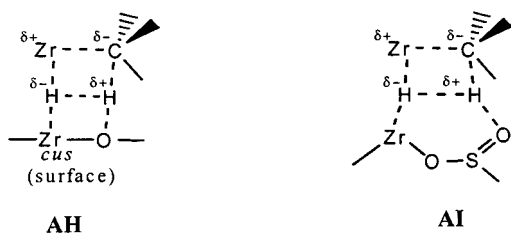(59) Lubben, T. V.; Wolczanski, P. T. *J. Am. Chem. Soc.* **1987**, *109* (2), 424–35.
(60) (a) Beswick, C. A.; Marks, T. J. *J. Am. Chem. Soc.* **2000**, *122* (42), 10358–10370, and references therein. (b) Horton, A. *Organometallics* **1996**, *15*, 2675–2677.
(61) Gill, R.; Petkovic, L. M.; Larsen, G. *J. Catal.* **1998**, *179* (1), 56–63.

(14a)

(14b)

L = THF or MeCN

(14c)

(not detected)

spectrum.[62] Such product signatures are not detected. Therefore, it is concluded that β-CH$_3$ elimination is not a major reaction pathway for **6**/ZRS400. These disparate features of homogeneous and heterogeneous neopentyl species suggest that the appreciable steric crowding on the surface (supported by the catalytic competence for high molecular weight polyolefin formation; vide supra) and possible electronic effects (presumably from surface oxygen) of the present system apparently inhibit significant β-CH$_3$ elimination (eq 14c).

Finally, it is conceivable that sulfated zirconia surfaces may participate in/facilitate Zr–C σ-bond hydrogenolysis via secondary interactions. While the H$_2$ molecule doubtless undergoes formal heterolytic cleavage in many homogeneous catalytic processes (interestingly, for Cp$'_2$Th(O^{t}Bu)CH$_2{}^t$Bu, the rate of σ-bond hydrogenolysis is accelerated in polar solvents[63]), there are also numerous reports[64] and theoretical analyses[65] of heterogeneous H$_2$ heterolytic chemisorption on oxide surfaces. Based on the suggested strong acid sites of sulfated zirconia (structures **I**−**M**), Lewis acid sites (*cus* Zr) are likely proximate to cationic organozirconium species, and *cus* Zr sites may stabilize four-center heterolytic transition states as in structure **AH**, an interaction supported by the observation of H$_2$ adsorption on the Lewis acid−base pairs of sulfated zirconia at low temperatures.[66]
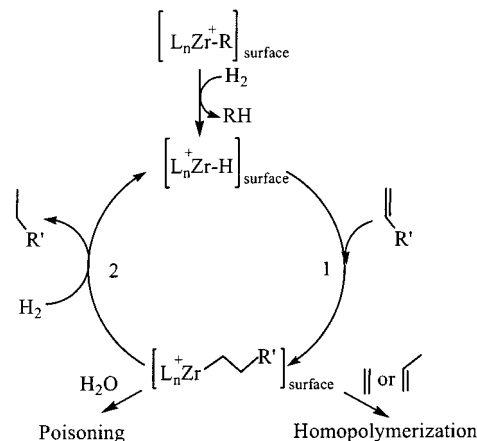
AH

AI

Recently, it has also been reported that H$_2$ molecules undergo heterolytic cleavage on the Zr–O–S=O sites to form Zr–H and S–OH groups.[67] On the basis of this observation, structure **AI** can be alternatively suggested.

(62) White, J. L.; Dias, A. J.; Ashbaugh, J. R. *Macromolecules* **1998**, *31* (6), 188−1888.

(63) $k_{THF}/k_{toluene}$ = 2.9(4). See: Lin, Z.; Marks, T. J. *J. Am. Chem. Soc.* **1987**, *109*, 7979−7985, and references therein.

(64) (a) Ioka, F.; Sakka, T.; Ogata, Y.; Iwasaki, M. *Can. J. Chem.* **1993**, *71* (5), 663−669. (b) Kazanskii, V. B. *Stud. Surf. Sci. Catal.* **1991**, *65*, 117−31, and references therein. (c) Ghiotti, G.; Boucuzzi, F.; Scala, R. *J. Catal.* **1985**, *92*, 79−97. (d) Lavalley, J. C.; Saussey, J.; Rais, T. *J. Mol. Catal.* **1982**, *17*, 289−298. (e) Mehta, S.; Simmons, G. W.; Klier, K.; Herman, R. G. *J. Catal.* **1979**, *57*, 339−346.

Scheme 1. Surface Chemistry and Catalytic Olefin Hydrogenation by Supported Organozirconium Complexes

II. Hydrogenation Mechanisms. In the simplest mechanistic scenario, steps 1 and 2 in Scheme 1 are assumed to be concerted and irreversible, and neither olefin nor H$_2$ is assumed to be coordinated to the metal ion of the active site during the catalytic cycle (such patterns in heterogeneous organothorium systems find parallels in homogeneous organothorium[19,68] and organolanthanide chemistry[23b,69]). Using the steady-state approximation, the rate of step 1 must be equal to that of step 2 and the overall conversion rate. The overall conversion rate, N_t, will then be related to k_1, k_2, and H$_2$ pressure as follows:

$$N_t = \frac{k_1 k_2 P_{H_2}}{k_1 + k_2 P_{H_2}} \qquad (15)$$

In previous work, the kinetic behavior of catalytic olefin hydrogenation mediated by Cp$'_2$Th(CH$_3$)$_2$/DA and its congeners was best described by eq 15.[6f] For these heterogeneous systems, neither olefin insertion (step 1 in Scheme 1) nor hydrogenolysis (step 2 in Scheme 1) is strictly turnover-limiting, the reaction of propylene with D$_2$ yields exclusively 1,2-propane-d_2, and activation energies are 3.6(2) and 5.3(2) kcal/mol for propylene and isobutylene hydrogenation, respectively.[6f] In the case of benzene hydrogenation by Th(allyl)$_4$/DA at 90 °C, P_{H_2} = 190 psi, the overall turnover frequency is zero-order in arene concentration and first-order in hydrogen pressure with an activation energy of 16.7(3) kcal/mol.[6d]
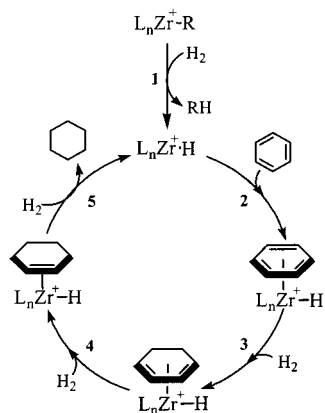
Mechanistic arguments for the present supported organozirconium catalysts begin by making several chemically reasonable assumptions: (1) the Zr center remains in the +4 oxidation state throughout the catalytic cycle (in analogy with the Th systems); (2) all catalytic steps take place at single Zr sites. The first assumption is supported by the fact that only $\sim$1 × 10^{-4} mol % of Zr sites in **3**/DA exist as ESR-detectable Zr-(III) species after He treatment and only ca. 3 × 10^{-2} mol % after H$_2$ treatment.[6g] Moreover, sulfated zirconia

(65) (a) Lukinskas, P.; Fărcaşiu, D. *Appl. Catal., A* **2001**, *209* (1, 2), 193−205. (b) Sutjianto, A.; Tam, S. W.; Pandey, R.; Curtiss, L. A.; Johnson, C. E. *J. Nucl. Mater.* **1995**, *219*, 250−258.

(66) Kostov, L. M.; Kazansky, V. B.; Figueras, F.; Tichit, D. *J. Catal.* **1994**, *150*, 143−149.

(67) Paukshtis, E. A.; Kotsarenko, N. S.; Shmachkova, V. P. *Catal. Lett.* **2000**, *69*, 189−193.

**Scheme 2. Plausible Mechanism for
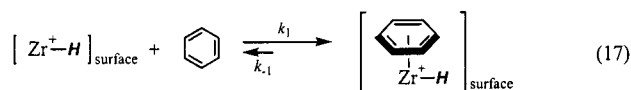[Zr$^+$−R]$_{surface}$-Catalyzed Arene Hydrogenation**

is known to be an oxidizing surface.[70] The second
assumption is reasonable in view of the large dispersion
of Zr sites (ca. 0.5 [Zr$_{active}$]/nm^2) and the relatively large
ZRS pore size (most frequent radius = ca. 35 Å).

One notable feature of the present catalyst systems
is the surprisingly high α-olefin and arene hydrogena-
tion activity. Complex **4**, which is more coordinatively
unsaturated/less sterically hindered than **3**, highlights
the reactivity among the ZRS-supported organozirco-
nium complexes employed in this study. Scheme 2
depicts a plausible mechanistic scenario for arene
hydrogenation and features sequences of precedented
stoichiometric transformations. Initially, benzene is
proposed to form an η^6 π-complex (η^6-arene cationic Zr
complexes are known[39a,71]). Every hydrogen addition
step is assumed to be sequential, affording precedented
η^4-[72] and then η^2-π complexes. The exact ancillary
ligation modes of the intermediate organozirconium
arene complexes cannot be fully specified with the data
at hand; however they may involve surface nucleophilic
centers (presumably surface oxygen atoms), as evi-
denced by a recent EXAFS study of silica- and alumina-
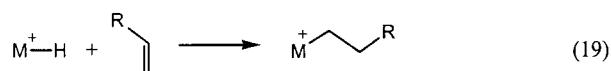supported zirconocenes.[40]

The kinetic study of **4**/ZRS400-mediated benzene
hydrogenation reveals that the rate law obeys eq 16.
Formation of an initial zirconium hydride arene complex
(step 1) is required to be rapid and essentially irrevers-

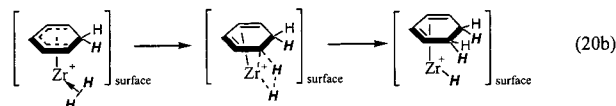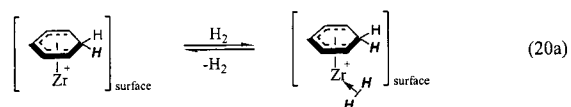$$N_t = k_{obs}[\text{arene}]^0 P_{H_2}{}^1 \qquad (16)$$

ible to form an intermediate π-complex and, subse-
quently, to yield an insertion product (eqs 17 and 18).
A reversible, concerted insertion mechanism, (e.g.,
without forming a discrete π-arene complex) cannot be

$$(17)$$

$$(18)$$

ruled out, and the present kinetic data do not rigorously
address the difference between the two mechanisms. In
the former scenario, k_1 must be much larger than k_2 to
exhibit zero-order kinetics in olefin concentration (eq
17). Equation 18 is a variant of an olefin insertion
reaction into an M−H bond (eq 19). Generally, olefin

$$(19)$$

insertion reactions are exothermic for group 4 transition
metal[73,74] and f-element hydrides,[75] in contrast to those
for later transition metals. For 1-butene insertion into
Zr−H and Hf−H bonds, ΔH_{ins} values are about −13
kcal/mol for Zr and −23 kcal/mol for Hf.[73] Furthermore,
eq 18 assumes polyhapto ligation after olefin insertion,
in which case ΔH_{ins} should be more negative.[73a] Next,
the presumed η^5-hexadienyl complex undergoes hydro-
genation and yields a (mono or di)ene Zr−H complex
(eqs 20a, 20b; step 3 in Scheme 2). The suggested four-
center transition state (eq 20b) has been frequently
proposed for early transition metal[76]/f-element metal[18,77]
catalyzed dihydrogen activation and is supported by
computational studies.[78]

$$(20a)$$

$$(20b)$$

For **4**/ZRS400-mediated benzene hydrogenation, the
first-order dependence on H$_2$ accommodates several
possibilities for the turnover-limiting step. One would
involve a turnover-limiting step in which a single H$_2$
molecule is simply added. A second possibility is that a

(68) (a) Bruno, J. W.; Strecher, H. A.; Morss, L. R.; Sonnenberger,
D. C.; Marks, T. J. *J. Am. Chem. Soc.* **1986**, *108*, 7275−7280. (b) Bruno,
J. W.; Marks, T. J.; Morss, L. R. *J. Am. Chem. Soc.* **1983**, *105*, 6824−
6832.

(69) (a) Giardello, M. A.; Conticello, V. P.; Brard, L.; Gagné, M. R.;
Marks, T. J. *J. Am. Chem. Soc.* **1994**, *116*, 10241−10254. (b) Jeske,
G.; Lauke, H.; Mauermann, H.; Schumann, H.; Marks, T. J. *J. Am.
Chem. Soc.* **1985**, *107*, 8111−8118.

(70) Ghenciu, A.; Fǎrcaşiu, D. *J. Mol. Catal. A: Chem.* **1996**, *109*,
273−283.

(71) (a) Chen, Y.-X.; Marks, T. J. *Organometallics* **1997**, *16*, 3649−
3657. (b) Jia, L.; Yang, X.; Stern, C. L.; Marks, T. J. *Organometallics*
1997, *16*, 842−857. (c) See also: Musso, F.; Solari, E.; Floriani, C.;
Schenk, K. *Organometallics* **1997**, *16*, 4889−4895.

(72) (a) Erker, G. *Acc. Chem. Res.* **2001**, *34* (4), 309−317, and
references therein. (b) Sinnema, P.-J.; Meetsma, A.; Teuben, J. H.
Organometallics **1993**, *12*, 184−189.

(73) (a) Moscardi, G.; Piemontesi, F.; Resconi, L. *Organometallics*
1999, *18* (25), 5264−5275. (b) Thorsaug, K.; Støvneng, J. A.; Rytter,
E.; Ystenes, M. *Macromolecules* **1998**, *31*, 7149−7165. (c) Prosenc, M.-
H.; Brintzinger, H.-H. *Organometallics* **1997**, *16*, 3899−3894.

(74) Schock, L. E.; Marks, T. J. *J. Am. Chem. Soc.* **1988**, *110*, 7701−
7715.

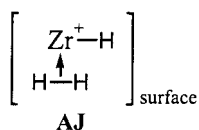(75) Lin, Z.; Marks, T. J. *J. Am. Chem. Soc.* **1990**, *112*, 5515−5525.

(76) (a) Guo, Z.; Bradley, P. K.; Jordan, R. F. *Organometallics* **1992**,
11, 2690−2693. (b) Thompson, M. E.; Baxter, S. M.; Bulls, A. R.;
Burger, B. J.; Nolan, M. C.; Santarsiero, B. D.; Schaefer, W. P.; Bercaw,
J. E. *J. Am. Chem. Soc.* **1987**, *109*, 203−219.

(77) Simpson, S. J.; Turner, H. W.; Andersen, R. A. *J. Am. Chem.
Soc.* **1979**, *101*, 7728−7729.

(78) (a) Kubas, G. J. In *Metal Dihydrogen and σ-Bond Complexes*;
Kluwer Academic/Plenum Publishers: New York, 2001; p 113. (b)
Ziegler, T.; Folga, E.; Berces, A. *J. Am. Chem. Soc.* **1993**, *115*, 636−
646. (c) Rabaâ, H.; Saillard, J.-Y.; Hoffmann, R. *J. Am. Chem. Soc.*
1986, *108*, 4327−4333. (d) Steigerwald, M. L.; Goddard, W. A., III. *J.
Am. Chem. Soc.* **1984**, *106*, 308−311. (e) Brintzinger, H. *J. Organomet.
Chem.* **1979**, *171*, 337−344.

rapid, reversible H_2 molecule addition is followed by some other turnover-limiting step. The latter scenario imposes significant constraints to satisfy the observed kinetic order, i.e., (1) the turnover-limiting step must not include a second H_2 addition coupled to the first rapidly reversible H_2 addition process, and (2) two or more coupled sequences of rapid/reversible H_2 addition cannot be part of the catalytic cycle, otherwise the observed P_{H_2} dependence would then be greater than first-order. All these considerations are based on the entirely reasonable assumption that arene initially binds the metal center as in eq 17.

Alternatively, it might be suggested that an H_2 molecule undergoes rapid, irreversible coordination to form an η^2-H_2 complex (structure **AJ**). Here, intramo-

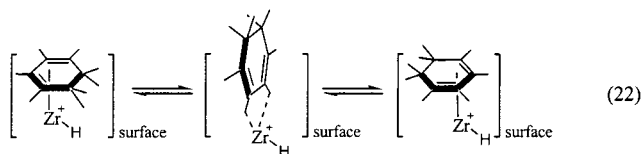$$\left[\begin{array}{c} Zr^+ \!\!-\! H \\ \uparrow \\ H \!\!-\! H \end{array} \right]_{surface}$$

AJ

lecular hydride transfers would then form reduced arene intermediates, and these process would be zero-order in P_{H_2}. Additional external H_2 would then be introduced in a later turnover-limiting step to conform to the observed kinetic results. A study of Cp'_2Eu-η^2-H_2, a rare d^0 η^2-H_2 complex, indicates that dihydrogen binding to such electrophilic metal centers is relatively weak and labile.[79] Considering the far greater concentration of arene present, which is also more basic than dihydrogen, this latter pathway seems less plausible. In the Arrhenius analysis of **6**/ZRS400, we make the physically reasonable assumption that the coverage of arene-bound metal species (eq 17) is constant over the measured temperature range (303.2−318.5 K). The observed E_a (10.3(8) kcal/mol) for **6**/ZRS400 is relatively low in comparison with the mean E_a range (∼6−22 kcal/mol) reported for conventional supported Ni arene hydrogenation catalysts.[51]

Regarding regiochemistry, evidence that H_2 units are delivered to the arene skeleton in a pairwise, *cis*-addition fashion has precedent in supported[47e,80] and homogeneous[81] early transition metal-catalyzed arene hydrogenation. Furthermore, previous olefin hydrogenation studies of homogeneous[75,82] and heterogeneous f-element hydrogenation catalysis,[6d,f] where H_2 addition is *cis*-1,2, are informative in understanding the present catalytic sequences. The presence of only two detectable $C_6D_6H_6$ regioisotopomers ($\alpha\alpha\alpha$ and $\alpha\alpha\beta$) in the present reaction mixtures supports the argument that (i) single

H_2 molecules are delivered to the same side of the carbocyclic ring as suggested in eqs 21a,b, and (ii) all H_2 deliveries are not to a single arene face. In addition, the isotopomer ratio ($\alpha\alpha\alpha$:$\alpha\alpha\beta$ = 1:3.1) argues that sequential suprafacial 1,2-H_2 additions to each olefin intermediate are essentially random (eq 21). Free,

$$\alpha\alpha\beta \equiv \alpha\beta\alpha \equiv \alpha\beta\beta$$
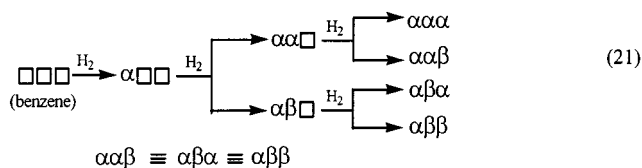
partially hydrogenated products are not detected during the course of the hydrogenation, suggesting two plausible scenarios. The first is that the partially hydrogenated olefinic species simply undergo dissociation and reassociation at the stages after steps 2 (diene complex) and 3 (olefin complex) in Scheme 2. Although partially hydrogenated products were not dectected, dienes and olefins are known have far higher binding affinities and undergo hydrogenation at far higher rates than arenes for homogeneous d^0-early transition metal catalysts[81] and supported organothorium catalysts.[6b] Therefore, the concentration of released diene or olefin will be very low in the steady-state regime. The second, alternative scenario is that the partially hydrogenated substrate remains in the Zr coordination sphere at all times but undergoes a change of Zr-coordinated face, presumably via agostic interactions (eq 22). In this case, the activa-

tion energy barrier must be low enough for the bound arene face to flip freely under the reaction conditions. This idea is supported by the characterization of analogous organozirconium diene flipping processes,[83] which are rapid on the NMR time scale above −80 °C.[83a]

Comparison to Other Homogeneous and Heterogeneous Catalyst Systems. Since the first discovery of arene hydrogenation catalysts, a wide range of homogeneous[81,84] and supported metal arene hydrogenation catalysts[6a,b,47] have been investigated. In general, the homogeneous catalysts reported to date have rela-

(79) Nolan, S. P.; Marks, T. J. *J. Am. Chem. Soc.* **1989**, *111*, 8538−8549.

(80) Huang, Y.; Profilet, R. D.; Ng, J. H.; Ranasinghe, Y. A.; Rothwell, I. P.; Freiser, B. S. *Anal. Chem.* **1994**, *66*, 1050−1055.

(81) (a) Burwell, R. L. *Chemtracts* **1998**, *11* (12), 884−892. (b) Rothwell, I. P. *J. Chem. Soc., Chem. Commun.* **1997**, 1331−1338, and references therein. (c) Parkin, B. C.; Clark, J. R.; Visciglio, V. M.; Fanwick, P. E.; Rothwell, I. P. *Organometallics* **1995**, *14*, 3002−3013. (d) Lockwood, M. A.; Potyen, M. C.; Steffey, B. D.; Fanwick, P. E.; Rothwell, I. P. *Polyhedron* **19XX** *14* (22), 3292−3313. (e) Yu, J. S.; Ankianiec, B. C.; Nguyen, M. F.; Rothwell, I. P. *J. Am. Chem. Soc.* **1992**, *114*, 1927−1929. (f) Ankioniec, B. C.; Fianwick, P. E.; Rothwell, I. P. *J. Am. Chem. Soc.* **1991**, *113*, 4710−4712.

(82) (a) Jeske, G.; Lauke, H.; Mauermann, H.; Swepston, P. N.; Schumann, H.; Marks, T. J. *J. Am. Chem. Soc.* **1985**, *107*, 8091−8103. (b) Jeske, G.; Lauke, H.; Schock, L. E.; Swepston, P. N.; Schumann, H.; Marks, T. J. *J. Am. Chem. Soc.* **1985**, *107*, 8103−8110. (c) Jeske, G.; Lauke, H.; Mauermann, H.; Schumann, H.; Marks, T. J. *J. Am. Chem. Soc.* **1985**, *107*, 8111−8118.

(83) (a) Pindado, G. J.; Thornton-Pett, M.; Bochmann, M. *J. Chem. Soc., Dalton Trans.* **1997**, 3115−3127. (b) Yasuda, H.; Kajihara, Y.; Mashima, K.; Nagasuna, K.; Lee, K.; Nakamura, A. *Organometallics* **1982**, *1*, 388−396.

(84) (a) Dyson, P. J.; Ellis, D. J.; Parker, D. G.; Welton, T. *Chem. Commun.* **1999**, 25−26. (b) Fidalgo, E. G.; Plasseraud, L.; Süss-Fink, G. *J. Mol. Catal. A Chem.* **1998**, *132*, 5−12. (c) Trzeciak, A. M.; Glowiak, T.; Ziolkowski, J. J. *J. Organomet. Chem.* **1998**, *552* (1−2), 159−164. (d) Ferrughelli, D. T.; Horváth, I. T. *J. Chem. Soc., Chem. Commun.* **1992**, *11*, 806−807. (e) Linn, D. E. Jr.; Halpern, J. *J. Am. Chem. Soc.* **1987**, *109*, 2969−2974. (f) Landis C. R.; Halpern, J. *Organometallics* **1983**, *2*, 840−842. (g) Bennett, M. A. *CHEMTECH* **1980**, 444−446, and references therein. (h) Muetterties, E. L.; Bleeke, J. R. *Acc. Chem. Res.* **1979**, *12*, 324−331, and references therein. (i) Bennett, M. A.; Huang, T.-N.; Turney, J. W. *J. Chem. Soc., Chem. Commun.* **1979**, 312−324. (j) Bennett, M. A.; Huang, T.-N.; Smith, A. K.; Turney, J. W. *J. Chem. Soc., Chem. Commun.* **1978**, 582−583. (k) Russell, M. J.; White, C.; Maitlis, P. M. *J. Chem. Soc., Chem. Commun.* **1977**, 427−428. (l) Feder, H. M.; Halpern, J. *J. Am. Chem. Soc.* **1975**, *97*, 7186−7188.

tively low activities, present difficulties in catalyst/ product separation, and in some cases have short catalyst lifetimes.[84b] Except for some d[0] catalysts,[6b] one-[84k] or two[84a,e,g–k] -electron oxidation state shuttling has been proposed for the catalytic cycles and, with the possible exception of Rothwell's $M(OAr)_3Cl_3/3^nBuLi$-based systems (M = Nb, Ta),[81] is in sharp contrast to the present group 4 or the previous f-element-based catalysts, which cannot readily access oxidative addition/reductive elimination sequences. Functional group tolerance is dependent on catalyst characteristics for both homogeneous and heterogeneous catalysts, and some recently developed homogeneous catalysts even exhibit excellent catalytic activities in aqueous media.[84a] Kinetic studies of several homogeneous arene hydrogenation systems indicate that rate laws are dependent on the particular catalyst system: in one case, the rate law is first-order in arene and zero-order in H_2,[84f] while in an other, it is first-order in arene–catalyst complex and first-order in H_2.[84e] In regard to benzene hydrogenation by conventional heterogeneous catalysts, rate laws are generally zero-order in arene and first-order in H_2.[50] While homogeneous catalysts ranging from early to mid-late transition metal complexes generally exhibit high regiospecificity[82,84g–k] (i.e., H_2 delivery to a single arene face), heterogeneous catalysts seldom exhibit exclusive single-face H_2 delivered products.[50] For both conventional homogeneous and heterogeneous arene hydrogenation catalysts, no olefin polymerization activity has been reported, and arene hydrogenation activities generally decrease with increasing ring substitution.[50,84h] The latter behavior is also observed with the present catalysts.

The structural study of the present catalyst system indicates that cationic, coordinatively unsaturated character in the organozirconium adsorbates is essential to catalytic activity. Interestingly, although there are several reports of olefin hydrogenation,[85] to date arene hydrogenation activity has not been reported for the homogeneous cationic group 4 complexes. That the present catalytic systems exhibit unprecedented arene reduction activities under ambient conditions underscores the remarkable synergistic effects arising from the interaction between the metal complex and surface functionalities.

Conclusions

Arene hydrogenation is a relatively demanding catalytic transformation that is not only of scientific interest but also of technological interest for aromatics reduction in fuel[86] and adipic acid production.[87] Therefore, it is remarkable that a straightforwardly prepared surface environment such as that of sulfated zirconia converts simple d[0] hydrocarbyl precursors into such highly active arene hydrogenation and olefin polymerization catalysts with a large percentage of the sites being catalytically active. The results of the present integrated structural, kinetic, and mechanistic study provide insights into surface chemistry and catalytic properties of organozirconium complexes chemisorbed on previously uninvestigated strongly Brønsted acidic surfaces. The ^{13}C CPMAS investigations combined with the selective ^{13}C-labeling techniques clearly demonstrate that the alkyl groups of organozirconium hydrocarbyls undergo protonolytic cleavage by surface hydroxy functionalities, resulting in highly electrophilic cationic adsorbate molecules. Interestingly, the present sulfated zirconia-supported organozirconium catalysts demonstrate rather similar trends in rate law, regiospecificity, and substrate reactivity as conventional metal hydrogenation catalysts, but with greater selectivity as a function of arene substituents. Furthermore, the CPMAS studies and high activities for olefin polymerization activities indicate that the present catalytic processes are molecule-based and highly sensitive to ancillary ligation. Further studies are in progress to probe the possibility of further enhancing catalytic activity by employing modified-sulfate zirconia as well as using other surface-modified metal oxide systems.

Supporting Information Available: Additional information as noted in text (schematic diagrams of reactor A and B, TGA graph of ZRS0, powder diffraction data for ZR and ZRS400 samples, and selected IR spectra of catalysts and supports). This material is available free of charge via the Internet at http://pubs.acs.org.

OM020056X

(85) (a) van Koten, G.; van Leeuwen, P. W. N. M. *Stud. Surf. Sci. Catal.* **1999**, *123*, 289–342, and references therein. (b) Rekonen, P.; Kopola, N.; Koskimies, S.; Andell, O. Makela, M. WO PCT Int. Appl. 95/25130. (c) Cuenca, T.; Flores, J. C.; Royo, P. *J. Organomet. Chem.* **1993**, *462* (1–2), 191–201. (d) Waymouth, R.; Pino, P. *J. Am. Chem. Soc.* **1990**, *112*, 2 (12), 4911–4914.

(86) For a review, see: Stanislaus, A.; Cooper, B. H. *Catal. Rev.-Sci. Eng.* **1994**, *36*, 75–123, and references therein.
(87) Parshall, G. W.; Ittel, S. D. *Homogeneous Catalysis*; John Wiley & Sons: New York, 1992; Chapter 7.5.